



저작자표시-비영리-변경금지 2.0 대한민국

이용자는 아래의 조건을 따르는 경우에 한하여 자유롭게

- 이 저작물을 복제, 배포, 전송, 전시, 공연 및 방송할 수 있습니다.

다음과 같은 조건을 따라야 합니다:



저작자표시. 귀하는 원저작자를 표시하여야 합니다.



비영리. 귀하는 이 저작물을 영리 목적으로 이용할 수 없습니다.



변경금지. 귀하는 이 저작물을 개작, 변형 또는 가공할 수 없습니다.

- 귀하는, 이 저작물의 재이용이나 배포의 경우, 이 저작물에 적용된 이용허락조건을 명확하게 나타내어야 합니다.
- 저작권자로부터 별도의 허가를 받으면 이러한 조건들은 적용되지 않습니다.

저작권법에 따른 이용자의 권리는 위의 내용에 의하여 영향을 받지 않습니다.

이것은 [이용허락규약\(Legal Code\)](#)을 이해하기 쉽게 요약한 것입니다.

[Disclaimer](#)

이학박사 학위논문

**Bimodal and multivariate analysis linking  
FDG uptake to BOLD signal at rest:  
a simultaneous hybrid PET/MR study**

휴지기 뇌 포도당 대사와  
BOLD 신호 관계에 관한  
다중모달리티 다변량 분석법:  
하이브리드 PET/MR 연구

2015년 8월

서울대학교 대학원

협동과정 인지과학 전공

김 은 경

**Bimodal and multivariate analysis linking  
FDG uptake to BOLD signal at rest:  
a simultaneous hybrid PET/MR study**

지도 교수 이 동 수

이 논문을 이학박사 학위논문으로 제출함  
2015년 4월

서울대학교 대학원  
협동과정 인지과학 전공  
김 은 경

김은경의 이학박사 학위논문을 인준함  
2015년 6월

위 원 장 김 청 택 (인)

부위원장 이 동 수 (인)

위 원 천 기 정 (인)

위 원 김 유 경 (인)

위 원 강 혜 진 (인)

# **Bimodal and multivariate analysis linking FDG uptake to BOLD signal at rest: a simultaneous hybrid PET/MR study**

**EunKyung Kim**

**Interdisciplinary Program in Cognitive Science  
The Graduate School**

A Thesis Submitted to the Faculty of Interdisciplinary Program  
in Cognitive Science, in Partial Fulfillment of the Requirements  
for the Degree of Doctor of Philosophy in Science  
at the Seoul National University, Seoul, Korea

June. 2015

Approved by thesis committee:

**Chairman** \_\_\_\_\_

**Vice-chairman** \_\_\_\_\_

**Member** \_\_\_\_\_

**Member** \_\_\_\_\_

**Member** \_\_\_\_\_

## **Abstract**

# **Bimodal and multivariate analysis linking FDG uptake to BOLD signal at rest: a simultaneous hybrid PET/MR study**

Eunkyung Kim

Interdisciplinary Program in Cognitive Science

The Graduate School

Seoul National University

Glucose consumption and hemodynamic response to neural activity at rest reflect intrinsic brain function in general. Investigating the relationship between them should be needed to better understand how the brain works. I applied the multivariate partial least squares for investigating the relationship between FDG uptake and BOLD signal at rest ( $n = 38$ , mean age  $44 \pm 13.9$  years), as representative measurements for capturing those different aspects of brain function using a hybrid PET/MR scanner. This approach can consider the interdependency between voxels as well as the relationship between modalities. As a

result, the relationship which was reproducible by a split-half resampling, was found in brain areas in respect to their functional roles. For example, the FDG uptake and BOLD signal showed positive relationship within the brain regions such as (1) sensory system, and (2) default mode network system. The negative relationship was found between the above regions.

The principal component analysis was also performed to investigate the interregional correlation patterns within modality. The first principal component image of FDG-PET was almost the same to the first singular image of FDG-PET. While, the first and second principal component images of fMRI were similar to the first singular image of fMRI. The first principal component image of fMRI represented the (1) visual system, and (2) default mode network system. The second principal component image of fMRI represented the (1) auditory and motor systems, and (2) default mode network system. The results proved that the interregional correlation patterns derived by the spontaneous ongoing neural activity were divided into the specialized independent systems compared to the interregional correlation patterns derived by the relatively stable FDG uptake.

This present work showed that the relationship between FDG uptake and BOLD signal was changed by age. By applying the partial least squares to the younger adults ( $n = 19$ , mean age  $32 \pm 6.9$  years) and

older adults groups ( $n = 19$ , mean age  $56 \pm 7.7$  years) respectively, the different relationship between FDG uptake and BOLD signal was observed. The changes of brain function due to aging can be observed by the changes of the relationship between FDG uptake and BOLD signal.

**Keywords:** FDG-PET, rsfMRI, partial least squares, multimodal, hybrid PET/MR, age

**Student Number:** 2011-30865

# Contents

<b>Abstract</b> .....	<b>i</b>
<b>Contents</b> .....	<b>iv</b>
<b>List of Figures</b> .....	<b>vii</b>
<b>List of Tables</b> .....	<b>ix</b>
<b>1. Introduction</b> .....	<b>1</b>
1.1. Multimodal and multivariate analyses of human brain .....	1
1.2. The relationship between FDG uptake and BOLD signal of the brain...	3
1.3. Investigating relationship between FDG uptake and BOLD signal by bimodal and multivariate PLS .....	6
<b>2. Materials and Methods</b> .....	<b>10</b>
2.1. Participants .....	10
2.2. Images scanning acquisition .....	12
2.3. Images preprocessing .....	15
2.3.1. FDG-PET images preprocessing .....	15
2.3.2. Functional MR images preprocessing .....	16

2.4. General approach and practical application of the partial least squares analysis .....	18
2.4.1. Partial least squares analysis – general approach .....	18
2.4.1.1. Procedures of partial least squares analysis .....	18
2.4.1.2. Significance test of singular images by a permutation method .....	20
2.4.1.3. Cross-validation of singular images by a split-half resampling.....	21
2.4.2. Partial least squares analysis – practical approach .....	28
2.5. Estimating principal component images of FDG-PET and fMRI .....	30
2.6. Partial least squares analysis applied to the younger adults and older adults groups .....	31
2.6.1. The effect of age to the significant latent variables.....	31
2.6.2. Partial least squares analysis .....	31
<b>3. Results .....</b>	<b>32</b>
3.1. The relationship between FDG uptake and BOLD signal .....	32
3.2. The reproducibility of the singular images .....	35
3.3. The principal component images of the FDG-PET and fMRI.....	40
3.4. The effect of age to the significant latent variables .....	46
3.5. The relationship between FDG uptake and BOLD signal in the younger adults and older adults groups .....	48

<b>4. Discussion.....</b>	<b>51</b>
4.1. Relationship between FDG uptake and BOLD signal at rest .....	51
4.2. The association of the singular images with the principal component images of FDG-PET and fMRI.....	55
4.3. The effect of age to the relationship between FDG uptake and BOLD signal.....	57
<b>5. Conclusion and limitations .....</b>	<b>60</b>
<b>References .....</b>	<b>63</b>
국문초록 .....	71

# Figures

Figure 1. PET/MRI imaging protocol and measurement schedule .....	14
Figure 2. Schematic representation of partial least squares analysis applied to the FDG-PET and fMRI data .....	23
Figure 3. Schematic representation of significance testing on singular values using a permutation method .....	25
Figure 4. Schematic representation of cross-validation testing using a split-half resampling .....	27
Figure 5. The spatial covariance patterns between FDG uptake and BOLD signal .....	33
Figure 6. The spatial covariance patterns between FDG uptake and BOLD signal using a split-half resampling.....	36
Figure 7. The reproducibility of the singular images between FDG uptake and BOLD signal using a split-half resampling.....	38
Figure 8. The percent contribution and visualization of significant principal component images of FDG-PET .....	41
Figure 9. The percent contribution and visualization of significant principal component images of fMRI.....	42

Figure 10. The agreement between the significant singular images and principal component images of FDG-PET .....43

Figure 11. The agreement between the significant singular images and principal component images of fMRI.....45

Figure 12. The relationship between age and FDG uptake or BOLD signal...47

Figure 13. The spatial covariance patterns between FDG uptake and BOLD signal in the younger adults and older adults groups .....49

# Tables

Table 1. Demographic data of participants.....	11
Table 2. Reproducibility of the singular images which have maximal relationship between FDG uptake and BOLD signal .....	39
Table 3. Similarity between the singular images of younger adults and older adults groups, which have maximal relationship between FDG uptake and BOLD signal measured by the <i>Pearson's</i> correlation coefficient .....	50

# 1. Introduction

## 1.1. Multimodal and multivariate analyses of human brain

Technical advances provide a chance to investigate the human brain *in vivo* using various imaging modalities. Each imaging modality enable to measure the brain at different points of views, depending on different time scales and spatial resolutions, or different data characteristics (see review of Horwitz and Poeppel, 2002, and Huster et al., 2012).

A lot of effort has been made to combine such multiple imaging modalities for better understanding of how the brain works. For example, enriched interpretations of human brain function in respect to the specific cognitive process are possible by combining functional magnetic resonance imaging (fMRI) and electroencephalography (EEG) (Iannaccone et al., 2015; Menon et al., 1997; Mulert et al., 2004). This kind of approach analyzes each modality independently and interprets the results together as a converging evidence.

It brings into question the general assumption that the brain signals measured by each modality correspond to the same set of underlying neural activity (Horwitz and Poeppel, 2002). Is there a real correspondence between different imaging modalities? Multimodal fusion data analysis can answer the question by demonstrating the shared

information and relationship between different aspects of the brain.

The representative multimodal fusion data analyses were listed in detail in the previous paper, including joint independent component analysis (jICA), multimodal canonical correlation analysis (mCCA), and partial least squares (PLS) (for a review, see Sui et al., 2012). The three multimodal fusion approaches have something in common. These are multivariate analyses in which interdependency between voxels is considered by assuming all brain voxels as a whole. Multivariate analyses have advantages over univariate analyses since the brain works as a system. In addition, these are data-driven analyses using blind source separation assuming linear mixtures of hidden sources. Different data sets can be combined together using a mathematical algorithm, and the hidden sources contributing to the relationship between different brain imaging data can be extracted successfully in the brain imaging studies.

Besides the common characteristics, the differences of such multimodal fusion data analyses make the each approach unique to the specific circumstance. For example, the jICA, which is the variation of independent component analysis (ICA) (Calhoun et al., 2006), has been used to find the independent component shared by different imaging modalities (Franco et al., 2008; Moosmann et al., 2008). It cannot find out the corresponding eigenvalue explaining contribution of the identified independent component to the data. The CCA, in contrast, has

been used to find the relationship between different data sets by maximizing correlation between them (Correa et al., 2010). The observed components are orthogonal with each other, and have the corresponding eigenvalue. The PLS is similar to the CCA analysis. It maximizes covariance between different data sets and assumes the linear relationship between independent and dependent variables.

## **1.2. The relationship between FDG uptake and BOLD signal of the brain**

Among multiple imaging modalities, [18F]fluorodeoxyglucose-positron emission tomography (FDG-PET) and fMRI are popular to measure human brain function. Convergent opinions have suggested that both two modalities measure the brain function in different ways (Raichle, 1998; Raichle, 2009; Strelnikov, 2010). FDG-PET measures FDG uptake which is closely related to the glucose metabolism reflecting relatively long-term and steady state neural activity. Glucose is a product of interaction between astrocyte and neuron (Bélanger et al., 2011). It is a substrate of neural energy requirement and related to the synaptic activity (Hertz and Zielke, 2004). Thus basis of neural activity can be detected by measuring glucose metabolism, and roughly by measuring FDG uptake. While, fMRI measures blood oxygenation level-dependent

(BOLD) signal reflecting relatively short-term and ongoing fluctuation of neural activity. BOLD signal is a product of complex interactions between blood flow, blood volume, and blood oxygenation (Ogawa et al., 1990; Ogawa et al., 1993). Thus indirect neural activity can be detected by measuring BOLD signal (Hyder et al., 2011).

These different characteristics of FDG-PET and fMRI often lead to independent use of each modality for understanding how the brain works. Nevertheless, the similar changes of FDG uptake and BOLD signal have been demonstrated in their response to the fundamental sensory processing (Newberg et al., 2005), despite the difficulty to obtain repeated measurements using the FDG-PET due to the relatively long half-life of  $^{18}\text{F}$  (Raichle, 2009). The brain energy demands have been also suggested as an important indicator to interpret the fMRI results (Hyder et al., 2002; Shulman et al., 2002; Shulman et al., 2004). In addition, the cerebral metabolism was tightly coupled with the functional connectivity derived from the BOLD signal at rest (Riedl et al., 2014). It suggested a close relationship between FDG uptake and BOLD signal regardless of different characteristics.

To understand the close relationship between FDG uptake and BOLD signal, recent studies have shown their spatial similarity using univariate analysis during resting state condition. The positive relationship between FDG uptake and BOLD signal was observed in

global brain in the 8 healthy adults (mean age  $34 \pm 10.6$  years) and 9 patients with temporal lobe epilepsy (Nugent et al., 2015). Regionally, the higher FDG uptake and higher BOLD signal were observed in the cerebellum, occipital, and parietal cortices, by the voxel-wise correlation analysis of 54 healthy adults (mean age  $36 \pm 12$  years) (Tomasi et al., 2013). The spatial similarity of brain activity was observed between the FDG uptake and BOLD signal fluctuation when the dorsal posterior cingulate cortex as a seed region in 8 healthy adults (mean age  $53 \pm 10.5$  years) (Passow et al., 2015).

These univariate analyses, however, cannot consider the interdependency between voxels. In addition, independent analysis cannot find the linear mixture of neural activity covaried with the FDG uptake and BOLD signal at the same time. Therefore, to better understand the close relationship between FDG uptake and BOLD signal, multimodal fusion data analysis should be applied. Among the multivariate analyses as I described earlier, PLS can find linkage shared by two different data (independent and dependent variables), based on their linear relationship (Krishnan et al., 2011; McIntosh et al., 1996). Intuitive understanding of the maximal relationship between FDG uptake and BOLD signal can be also possible by visualizing the identified components on to the brain.

### **1.3. Investigating relationship between FDG uptake and BOLD signal by bimodal and multivariate PLS**

The aim of this present work was investigating relationship between FDG uptake and BOLD signal of the brain using bimodal and multivariate analysis. The PLS was applied to the resting state FDG-PET and fMRI data of 38 healthy adults (mean age  $44 \pm 13.9$  years). The FDG-PET and fMRI data were acquired by a hybrid PET/MR scanner. It allows simultaneous acquisition of FDG-PET and functional MR images, providing complementary information for the functional brain changes (Heiss, 2009; Wehrl et al., 2014).

Traditionally, the PLS has been used to find the brain areas related to the experimental contrast or behavioral outcome (McIntosh et al., 1996), and used to find the relationship between different brain imaging modalities (Burzynska et al., 2013; Chen et al., 2009). For example, the relationship between white matter integrity and BOLD signal during working memory task was investigated (Burzynska et al., 2013). The relationship between FDG uptake and gray matter volume was also investigated by the PLS (Chen et al., 2009).

In this present work, I focused on the relationship between FDG uptake and BOLD signal at rest, without any specific task. The advantage of resting state study is simplicity with reliable findings (Ferreira and Busatto, 2013), germane to the task-related brain activity (Hasson et al.,

2009; Lewis et al., 2009). In fact, the energy consumption supporting brain activity at rest is remarkably large compared to the one associated with changes in brain activity (see review of Raichle, 2010). The reason why this large amount of energy at rest is needed is unclear, but acquisition and maintenance of information may be the possible causes (see review of Raichle, 2010). Therefore, investigation of functional brain imaging acquired during resting state condition provides invaluable information for the fundamental understanding of the brain, rather than understanding of brain activity in response to external stimuli. In this regard, investigation of the relationship between FDG uptake and BOLD signal at rest can reflect the balance of long-term and stable brain signal with the spontaneous brain activity to maintain the normal brain function.

The linkage between FDG uptake and BOLD signal was extracted by applying the PLS to the resting state FDG-PET and fMRI data in healthy adults. A split-half resampling was performed to validate the findings. The relationship might be different to the previous studies reporting spatial similarity and positive association between them (Nugent et al., 2015; Passow et al., 2015; Tomasi et al., 2013). For example, the relationship between FDG uptake in one brain region and the BOLD signal in other brain areas where have different roles of functional processing, could be observed as a negative way. It was

reasonable according to the previous study reporting the negative relationship between different brain areas, processing externally and internally oriented stimuli using resting state fMRI data (Tian et al., 2007). In addition, the FDG uptake and BOLD signal of similar brain areas might not show the spatial similarity or positive relationship, according to the previous study reporting their mismatched activity to the whisker-stimulation of rats (Wehrl et al., 2014).

To better understand the relationship between FDG uptake and BOLD signal, I also obtained the principal component images of FDG-PET and fMRI, respectively. The principal component images of each modality can explain the interregional correlation patterns of resting state FDG uptake and BOLD signal itself, rather than the interactions between modalities. In other words, the patterns of principal component images of each modality are independent to the patterns of singular images depicting the interrelationship between modalities, and represent the distributed brain systems in which high intercorrelations are observed (Friston et al., 1993). By comparing the principal component images and the singular images of each modality, the contribution of each modality to their relationship was revealed in this present work.

In addition, I also divided the participants into younger adults ( $n = 19$ , mean age  $32 \pm 6.9$  years) and older adults groups ( $n = 19$ , mean age  $56 \pm 7.7$  years), and investigated the effect of age to the relationship

between FDG uptake and BOLD signal at rest. Since age affects to the brain function significantly, it is reasonable to infer that the relationship between FDG uptake and BOLD signal might be changed depending on age. According to the previous study, age was an important indicator to discriminate the relationship between different imaging modalities using the PLS (Chen et al., 2009).

## 2. Materials and Methods

### 2.1. Participants

Thirty eight healthy subjects (M/F: 19/19, mean age  $44 \pm 13.9$  years) participated in this study. Neuropsychological screening was tested to all volunteers, and the participants were included in this study according to the objective rules: Korean version of Mini-Mental State Examination (K-MMSE)  $\geq 27$  scores, Mood Evaluation Scale (MES)  $< 18$  scores, Beck Depression Inventory (BDI)  $\leq 9$  scores, and Beck Anxiety Inventory (BAI)  $\leq 7$  scores (Table 1). All participants were right-handed, and had no previous history of neurological or psychiatric disorder. The participants were divided into younger adults (M/F: 10/9, mean age  $32 \pm 6.9$  years) and older adults groups (M/F: 9/10, mean age  $55.5 \pm 7.7$  years) ( $P < 8.3E-012$ ). There was no significant difference between all the screening tests scores of two groups ( $P > 0.05$ ). This study was approved by the institutional review board (IRB) of the Seoul National University College of Medicine. They gave informed consent as provided by the Seoul National University Hospital.

**Table 1. Demographic data of participants**

Group	N(M/F)	Age		K-MMSE	MES	BDI	BAI
		mean	range (min, max)				
Younger adults	19 (10/9)	32 years	22 ~ 42 years	29.5 ± 0.8	4.5 ± 4.2	2.4 ± 2.4	1.9 ± 1.7
Older adults	19 (9/10)	56 years	46 ~ 71 years	29.1 ± 1.0	4.2 ± 2.5	3.6 ± 2.6	2.5 ± 2.0

## 2.2. Images scanning acquisition

All FDG-PET and MR images were acquired simultaneously using a Siemens Biograph mMR 3T scanner (Siemens Healthcare Sector, Germany). The measurement schedule for simultaneous PET/MR acquisition was visualized in Figure 1. The FDG-PET and fMRI were started to scan at the same time. FDG-PET images were acquired by list-mode acquisition, when 40 minutes after injection of FDG tracer ( $[^{18}\text{F}]$  FDG 5-7 mCi). The actual acquisition of FDG-PET images was started when 50~60 minutes after FDG administration according to the measurement schedule. In the previous studies, the 60 minutes interval between FDG administration and scanning was recommended (Boellaard et al., 2010) in which plateau concentrations were achieved (see review of Schmidt et al., 1996).

Scanning parameters of FDG-PET images, T2\*-weighted echo-planar images (EPI), and structural T1 images were as followings: FDG-PET: 127 slices covering the whole brain with transverse acquisition (matrix size,  $344 \times 344$ ; voxel size,  $1.04 \times 1.04 \times 2.03$ ); FOV=300mm; EPI: the number of total volume per one subject was 116 with mosaic image format; 35 slices covering the whole brain with interleaved acquisition (matrix size,  $128 \times 128$ ; voxel size,  $1.88 \times 1.88 \times 3.5$ ); TR=3500ms; TE=30ms/angle,  $90^\circ$ ; FOV=240mm; structural T1 images: spoiled grass gradient recalled (SPGR) 3D MRI sequence; 208 slices

covering the whole brain with sagittal acquisition (matrix size,  $256 \times 256$ ; voxel size,  $0.98 \times 0.98 \times 1$ ); TR=1670ms; TE=1.89ms; FOV=250mm. All images were acquired in a resting state condition (dimmed light, closed eyes, and without any task).

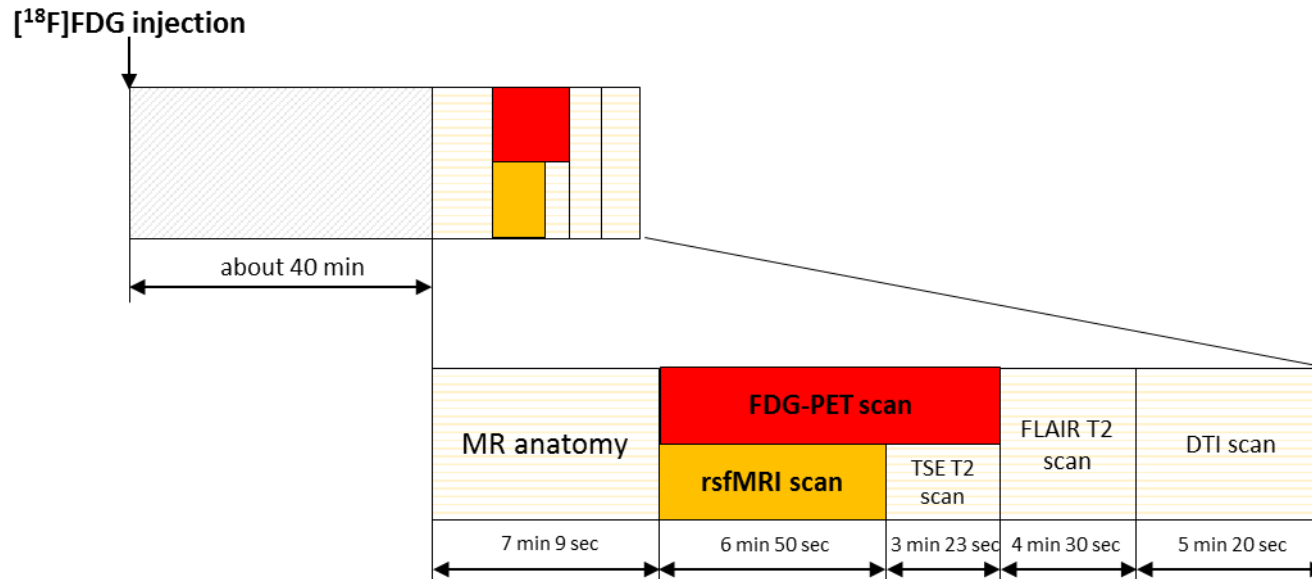


**Figure 1. PET/MRI imaging protocol and measurement schedule.** After injection of  $^{18}\text{F}$  FDG, participants rested in a quiet room for about 40 minutes and were moved into the PET/MR scanner. Structural MR images were acquired first. FDG-PET and fMRI were started to scan at rest at the same time by following T2 and DTI scan.

## **2.3. Images preprocessing**

### *2.3.1. FDG-PET images preprocessing*

FDG-PET images were preprocessed using the Statistical Parametric Mapping (SPM8, [www.fil.ion.ucl.ac.uk/spm](http://www.fil.ion.ucl.ac.uk/spm)) and PVElab software (Quarantelli et al., 2004). The obtained PET images were rescaled to  $256 \times 256$  matrix and coregistered to the T1 images. The coregistered PET images were corrected for partial volume effect, mainly due to low spatial resolution, using the modified version of Muller-Gartner approach (Muller-Gartner et al., 1992). To estimate the white matter value by the Rousset method (Rousset et al., 1998), the T1 images were segmented and resliced. The corrected PET images were spatially normalized to the Montreal Neurological Institute (MNI) with voxel resolution of  $2\text{mm}^3$ , and smoothed with 12mm FWHM. The images were masked by the gray matter tissue prior map provided in SPM8, excluding cerebellum cortex, thresholded at probability  $> 0.3$ . The image intensity was rescaled by global normalization to 50. The images obtained during the processing steps were visually confirmed to avoid any potential biases.

### 2.3.2. *Functional MR images preprocessing*

Functional MR images were preprocessed using the AFNI (Cox, 1996) and the FSL (Smith et al., 2004) by following procedures: 1) the first 4 volumes were discarded to eliminate the T1 relaxation effects and to enhance the BOLD signal stabilization; 2) despiking the signal from the time-series data to make the motion parameters were less variable and to suppress the signal due to the potential hardware instability (Jo et al., 2013); 3) head motion correction of fMRI volumes as the middle volume was the reference, using six degrees of freedom rigid body registration (Jenkinson et al., 2002); 4) slice timing correction for interleaved slice acquisition; 5) within run intensity normalization to a whole brain mode value of 1000 (Power et al., 2012); 6) spatial normalization of the functional MR images to the standard template with voxel resolution of  $2\text{mm}^3$ ; 7) spatial smoothing with FWHM 6mm. Non-brain voxels were removed by masking the brain using BET (part of prestats procedures in FEAT toolbox) to obtain the within run intensity values of whole brain voxels. The spatial normalization and spatial smoothing were performed using the SPM8. The nuisance variables including the average values of cerebrospinal fluid, gray matter, white matter, and the six motion parameters were regressed out using the general linear model. After that, the functional MR images were bandpass filtered ( $0.01 < f < 0.1$  Hz). The images were masked by the

gray matter tissue prior map provided in SPM8, excluding cerebellum cortex, thresholded at probability  $> 0.3$ .

Recently, the effort to remove the motion effect to the BOLD signal has been increased, since head motion, which is not eliminated by using six motion parameters, can bias the BOLD signal (Power et al., 2012). As one of the possible solutions for removing the motion effect, the framewise displacement (FD) and root mean square (RMS) variance of the temporal derivative (DVARs; the rate of changes of BOLD signal across the entire brain at each frame of data) were suggested in the previous study (Power et al., 2012). Generally, the criteria of FD and DVARs were suggested as follows:  $FD < 0.5$  mm and  $DVARs < 0.5$  % (Power et al., 2012). The FD was estimated after the slice timing correction. The DVARs was estimated using the final preprocessed functional MR images (after smoothing) to control the biased BOLD signal fluctuations. Once the volumes where signal was likely contaminated by motion or fluctuation were detected, the contaminated volumes and the surrounding volumes before 1 TR and after 2 TR were discarded, before performing analyses. This volume censoring technique was called ‘scrubbing’, and it was effective to identify and remove the motion effect, contaminating the BOLD signal. The FD and DVARs of the all participants were estimated. There was no participant above the criterion.

## **2.4. General approach and practical application of the partial least squares analysis**

In order to investigate the relationship between FDG uptake and BOLD signal, the PLS was applied to the resting state FDG-PET and fMRI data. The preprocessed images were used as input data. To avoid the computational burden due to the large variables (i.e., voxels in this case), singular value decomposition was performed by matrix transformation. The general approach of PLS and its practical application were described as follows.

### *2.4.1. Partial least squares analysis – general approach*

#### 2.4.1.1. Procedures of partial least squares analysis

The basic and most important assumption underlying the PLS in this study was that FDG uptake and BOLD signal of the brain shared some common features induced by neural activity. To extract the features, maximizing the covariance between FDG uptake and BOLD signal was needed. For this, data matrix of the functional MR images (subjects  $\times$  voxels  $\times$  time series) should be reduced to have the same dimension of the FDG-PET images (subjects  $\times$  voxels). Individual analyses (one-sample  $t$ -tests) were performed for each subject of fMRI data using the preprocessed images. The null hypothesis of individual analyses was that the BOLD signal amplitude was zero across the times series. The

outcome  $t$ -maps of individual analyses were transformed to  $z$ -maps to normalize subject variance.

After that, correlation between columns of  $X$  and  $Y$  could be estimated, where  $X$  indicated the concatenated matrix of FDG uptake of all brain regions over all individuals, and  $Y$  indicated the concatenated matrix of BOLD signal of all brain regions over all individuals. The  $X$  was independent variable and  $Y$  was dependent variable, according to the hypothesis of this study. The  $X$  and  $Y$  were rescaled as the mean of each column was zero and its sum of squares was one.

$$R = Y^T X$$

The correlation matrix  $R$  was then decomposed into three components, weighted matrix of BOLD signal ( $U$ ), singular value matrix ( $S$ ), and weighted matrix of FDG uptake ( $V$ ), using singular value decomposition. The column vectors of  $U$  and  $V$  were also called as singular vectors. The singular vector of each modality corresponding with the first singular value represented the information explaining maximal relationship between FDG uptake and BOLD signal.

Latent variables (LVs) were estimated by multiplying  $X$  and  $Y$  with corresponding singular vectors. The LVs of each dataset represented maximal relationship between FDG uptake and BOLD signal which

were projected on a new space. After that, singular images were reconstructed by multiplying the LVs with the X or Y. The singular images can be used to visualize the spatial pattern of the information on the brain space containing relationship between modalities. For example, the first singular image of each modality represented the information explaining maximal relationship between FDG uptake and BOLD signal. The schematic representation of PLS applied to the FDG-PET and fMRI data at rest was displayed in Figure 2.

#### 2.4.1.2. Significance test of singular images by a permutation method

To prove that the relationship between FDG uptake and BOLD signal of the brain was not noise but meaningful phenomenon, the significance of each singular image (equal to the significance of LVs, and the significance of each singular value) was tested and visualized in the following steps using a permutation test (Figure 3).

The pseudo X was generated by randomly reordered observations while Y was remained the same (Krishnan et al., 2011). Singular values were estimated by singular value decomposition after estimating the correlation matrix of the pseudo X and the Y. The above procedures repeated 1000 times and the estimated pseudo singular values were used for null distributions. If the observed singular value was larger

than the pseudo singular value (in this case,  $P < 0.005$ ), the corresponding singular images could be considered as significance. Multiple comparison correction was not needed since statistical test was performed in a single analytic step. The significant relationship between modalities was visualized by reconstructing singular image of each modality.

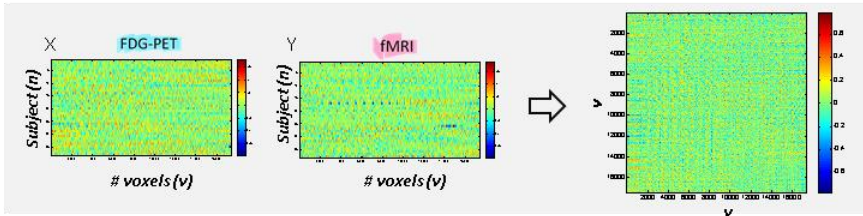
#### 2.4.1.3. Cross-validation of singular images by a split-half resampling

The PLS can find linkage shared by different data sets, so the singular images observed in this work might not be reproducible if the data was changed. To test the reproducibility of singular images, the participants were random split: half of the participants were treated as training data set and the other half were treated as test data set (Figure 4). The PLS was applied to the training data set and test data set, respectively. The significance of each singular image was tested by a permutation method (1000 times).

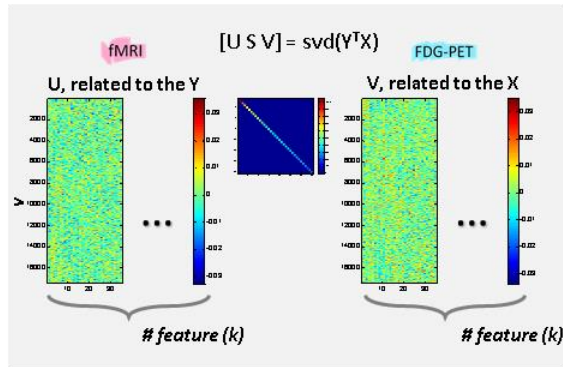
Once the significant singular images had been identified, reproducibility of the singular images was measured by *Pearson's* correlation coefficient. The significant singular images obtained in the test data set were compared to the one in the training data set by *Pearson's* correlation coefficient. If the *Pearson's* correlation coefficient

was above the certain threshold, there was agreement between singular images of training and test data sets. Generally, the following interpretation was suggested:  $r < 0.3$  indicated small correlation,  $0.3 < r < 0.5$  indicated moderate correlation,  $r > 0.5$  indicated large correlation (Cohen, 1988).

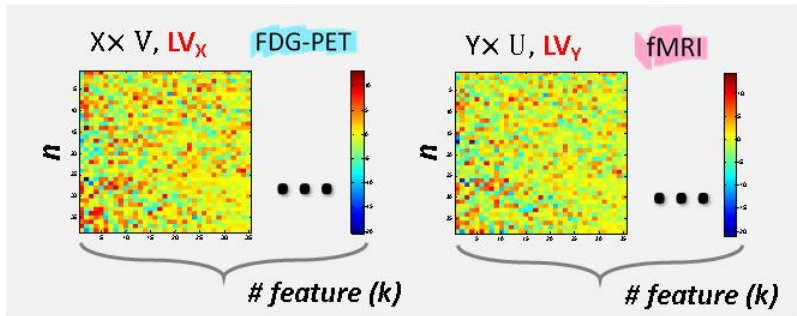
## A. Estimating correlation matrix, $Y^T X$



## B. Singular value decomposition



## C. Estimating latent variable



## D. Reconstruction data (singular images)

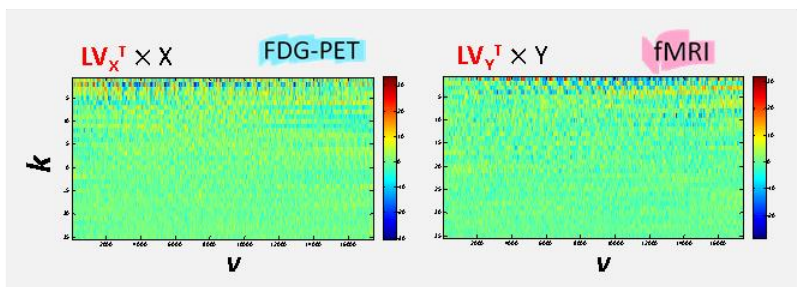


**Figure 2. Schematic representation of partial least squares analysis applied to the FDG-PET and fMRI data.** (A) The correlation between columns of  $X$  and  $Y$  was estimated, where  $X$  indicated the concatenated matrix of FDG uptake of all brain regions over all individuals, and  $Y$  indicated the concatenated matrix of BOLD signal of all brain regions over all individuals. The  $X$  and  $Y$  were rescaled as the mean of each column was zero and its sum of squares was one. (B) By using singular value decomposition, the correlation matrix was decomposed into three components, weighted matrix of BOLD signal ( $U$ ), singular value matrix ( $S$ ), and weighted matrix of FDG uptake ( $V$ ). (C) The latent variable (LV)s were estimated by multiplying  $X$  and  $Y$  with corresponding singular vectors. (D) The singular images were constructed by multiplying the  $X$  and  $Y$  with the corresponding LVs.

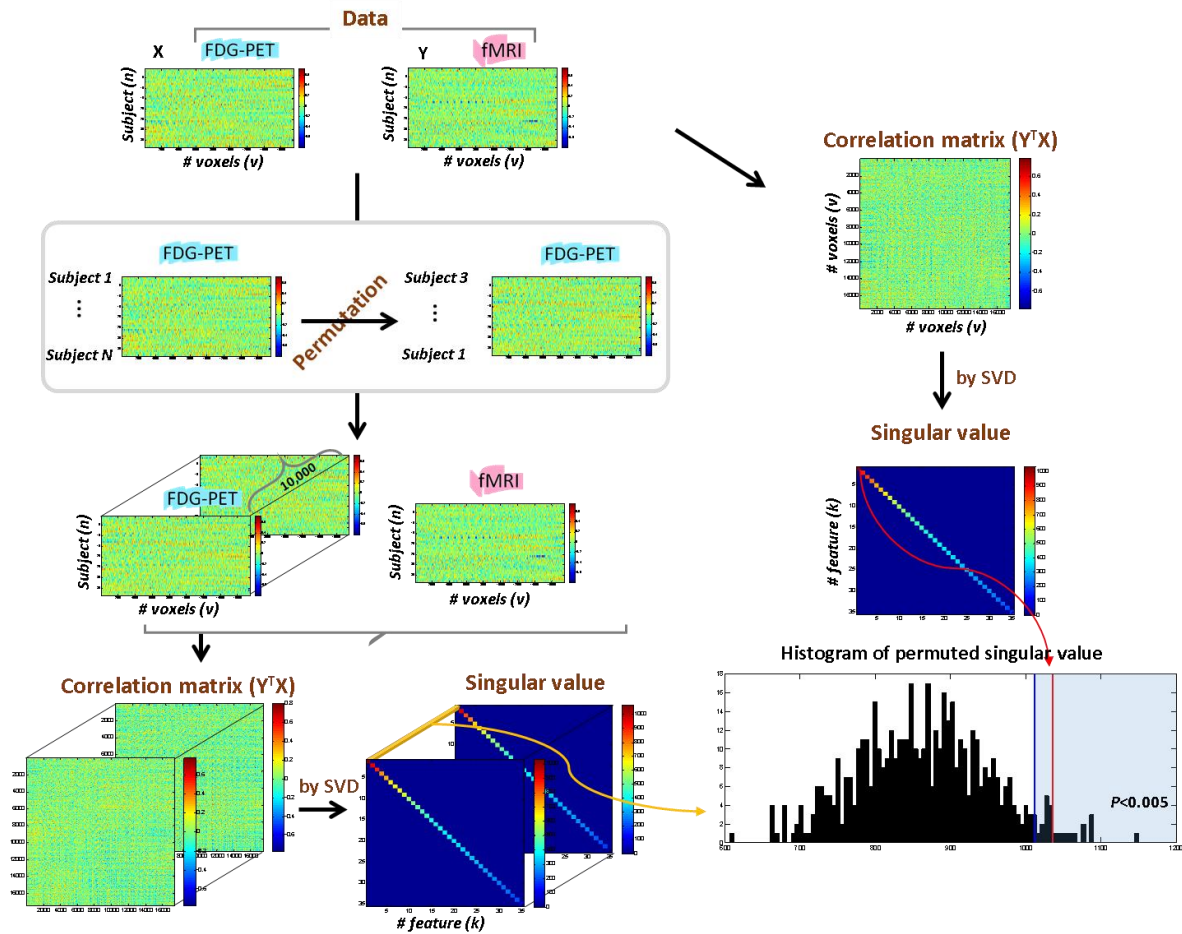


**Figure 3. Schematic representation of significance testing on singular values using a permutation method.** The significance of each vector of LVs containing information about the multivariate patterns of brain signal was tested using a permutation method. The X and Y represented FDG uptake and BOLD signal of all brain regions over all individuals. The permuted X was generated by randomly switching the order of individuals in the X. Then the correlation matrix was constructed by multiplying the Y with permuted X, and the singular value was estimated by singular value decomposition. This procedure was repeated 1000 times. The singular value from the permuted data was used as a null distribution. Probability that the observed singular value exceeded the permuted one was estimated. The significance was set at  $P < 0.005$  in this study.

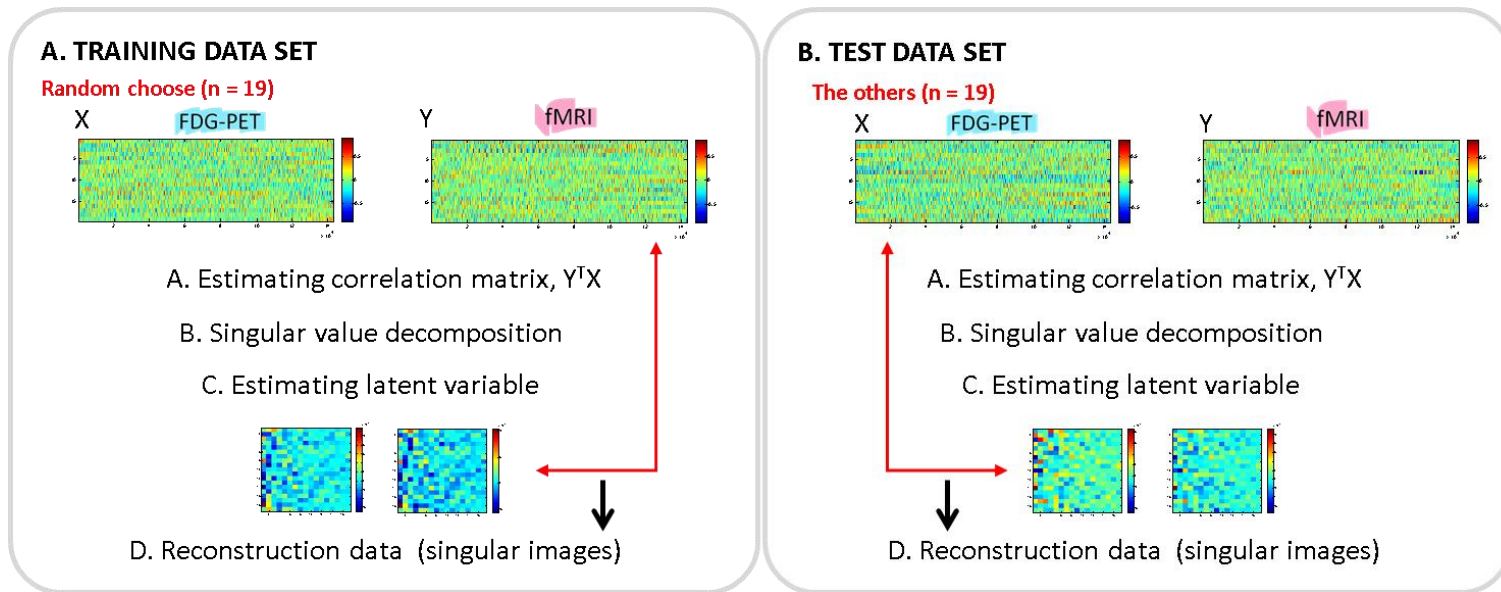


**Figure 4. Schematic representation of cross-validation testing using a split-half resampling.** The reproducibility of singular images was tested using a split-half resampling. (A) Half of the participants were randomly chosen as training data set and (B) the other half were treated as test data set. Singular images were estimated in each data set using the PLS. The reproducibility of a singular images was measured by the *Pearson's* correlation coefficient between the singular images of training and test data sets.

### 2.4.2. Partial least squares analysis – practical approach

The main disadvantage of PLS applied to this bimodal data was computational burden due to huge voxel size. For efficient processing, a computationally efficient method can be applied (Chen et al., 2009). According to the previous paper, eigenvector of  $X^TYY^TX$  is transposed to the  $A^TA$ , by following equations.

$$\Omega = X^TYY^TX = X^TZ^TZX = (ZX)^TZX = A^TA,$$

where  $A = ZX$ . If the  $V_1$  is an eigenvector of huge matrix  $A^TA$  with eigenvalue  $\alpha$ , eigenvector of smaller matrix  $AA^T$  is  $AV_1$ , following equations.

$$A^TAV_1 = \alpha V_1$$

$$AA^TAV_1 = \alpha AV_1$$

Conversely, if the  $V_2$  is an eigenvector of smaller matrix  $AA^T$  with eigenvalue  $\alpha$ , eigenvector of huge matrix  $A^TA$  is  $A^TV_2$ , by following equations.

$$AA^TV_2 = \alpha V_2$$

$$A^TAA^TV_2 = \alpha A^TV_2$$

Therefore  $A^T V_1$  is corresponded to the singular vectors for FDG-PET ( $X$ ). The eigenvector of  $A^T A$  is called as  $w_1$ . The latent variable of  $X$ , which is called as  $t_1$  can be computed by multiplying  $X$  with  $w_1$ . The singular vectors for fMRI ( $Y$ ), which is called as  $c_1$  can be computed by multiplying  $Y^T$  with  $t_1$  and divided by square root of eigenvalue. The latent variable of  $Y$ , which is called as  $u_1$ , can be computed by multiplying  $Y$  with  $c_1$ .

In practice, FDG-PET and fMRI data controlled gender effect by general linear model, were rescaled as the mean of each column was zero and its sum of squares was one. After that, the variable of  $w_1$  (corresponding to the singular vectors of  $X$ , in this case, FDG-PET),  $c_1$  (corresponding to the singular vectors of  $Y$ , in this case, fMRI),  $t_1$  (corresponding to the latent variable of  $X$ ),  $u_1$  (corresponding to the latent variable of  $Y$ ), and the singular values were estimated. Significance of each singular value was tested by random permutation (1000 times). All resampling data which may cause axis rotation or reflection was controlled by Procrustes rotation (McIntosh and Lobaugh, 2004; Milan and Whittaker, 1995).

## 2.5. Estimating principal component images of FDG-PET and fMRI

The principal component images of each modality represented the distributed brain system in which high interregional correlations were observed (Friston et al., 1993). In this framework, the interregional correlation patterns of FDG uptake or BOLD signal can be shown and compared to the singular images from the PLS, which showed the maximal relationship between modalities.

The procedure of principal component analysis was almost the same to the PLS analysis. The correlation matrix of FDG-PET (i.e., PET-to-PET) and fMRI (i.e., fMRI-to-fMRI) was estimated respectively, and decomposed by singular value decomposition (McIntosh et al., 1996; Worsley et al., 2005).

Since the majority of FDG uptake and BOLD signal can be explained by only using a few components, the significance of each principal component was tested by a permutation method (1000 times). After that, the similarity between the significant principal component images and the significant singular images was measured by estimating the *Pearson's* correlation coefficient. Generally,  $r < 0.3$  indicated small correlation,  $0.3 < r < 0.5$  indicated moderate correlation,  $r > 0.5$  indicated large correlation between the principal component images and singular images (Cohen, 1988).

## **2.6. Partial least squares analysis applied to the younger adults and older adults groups**

### *2.6.1. The effect of age to the significant latent variables*

The LVs such as t1 and u1, showed the maximal relationship between the modalities. The relationship can be accounted by age, because it leads to functional brain changes. The *Pearson's* correlation coefficient between age and the significant LVs was estimated to examine the effect of age. In addition, the LVs of 38 individuals were divided into younger and older adults groups and compared by using a two-sample *t*-test.

### *2.6.2. Partial least squares analysis*

The relationship between FDG uptake and BOLD signal of younger adults and older adults groups was estimated by the PLS, respectively. Significance of each singular value was tested by random permutation (1000 times). The significant singular images of each group were compared to find out the similarity between younger adults and older adults groups, by estimating the *Pearson's* correlation coefficient.

## **3. Results**

### **3.1. The relationship between FDG uptake and BOLD signal**

The spatial covariance patterns which have significant maximal relationship between FDG uptake and BOLD signal were found in the first three components for the FDG-PET and fMRI, respectively ( $P < 0.005$ , Figure 5). Each of the three pairs of singular images accounted for 30.4%, 22.5%, and 8.4% of the correlation matrix (i.e., correlation between FDG uptake and BOLD signal).

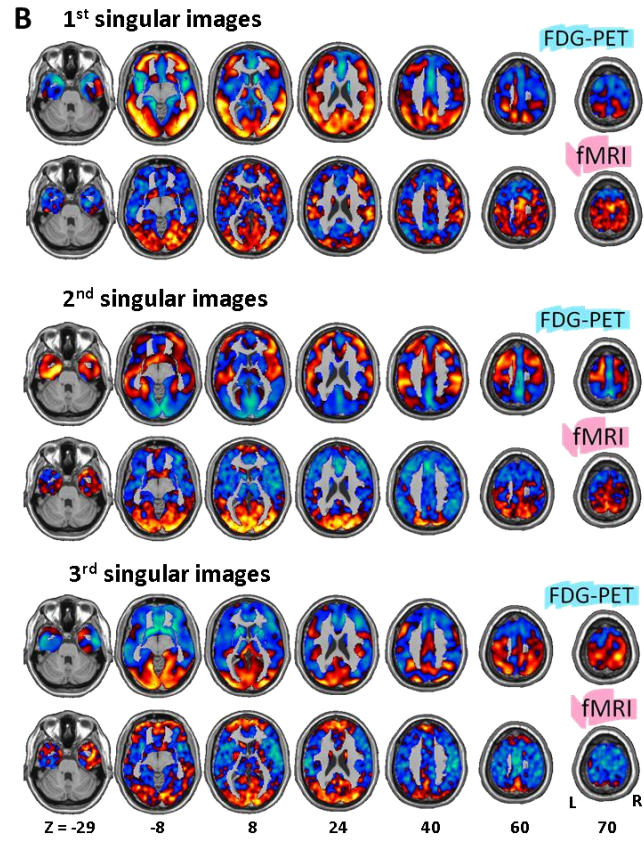
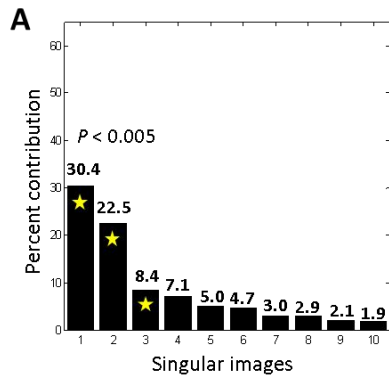


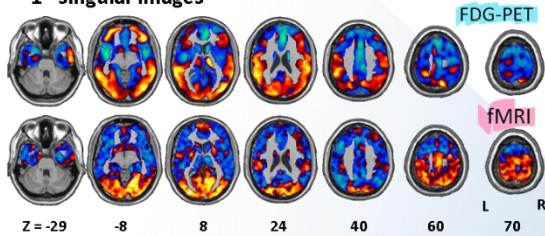
**Figure 5. The spatial covariance patterns between FDG uptake and BOLD signal.** (A) Scree plot of singular images representing the spatial covariance patterns between FDG uptake and BOLD signal. The x-axis indicate the singular images and the y-axis indicate the percent contribution. The significance of singular images was symbolized by a star mark (\*). (B) The 1<sup>st</sup> singular images, 2<sup>nd</sup> singular images, and 3<sup>rd</sup> singular images showed significant covariance patterns which were not noise, by random permutation test.

### 3.2. The reproducibility of the singular images

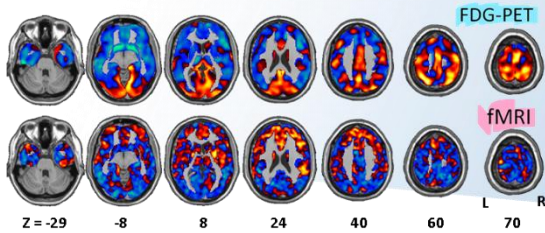
Among the significant singular images, the 1<sup>st</sup> singular images between FDG uptake and BOLD signal were consistently observed using a split-half resampling.

By using the training data set, the spatial covariance patterns which have significant maximal relationship between modalities were found in the first two components for the FDG-PET and fMRI, respectively ( $P < 0.005$ , Figure 6A). By using the test data set, the spatial covariance patterns which have significant maximal relationship between modalities were also found in the first two components for the FDG-PET and fMRI, respectively ( $P < 0.005$ , Figure 6B). Among them, the 1<sup>st</sup> singular images of test data set were similar to the 2<sup>nd</sup> singular images observed in the training data set ( $r = 0.48$  for the singular image of FDG-PET, and  $r = 0.37$  for the singular image of fMRI, Figure 7, Table 2).

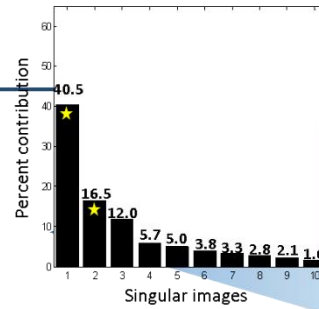
### 1<sup>st</sup> singular images



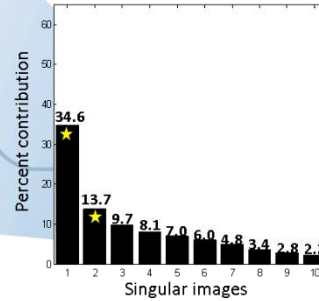
### 2<sup>nd</sup> singular images



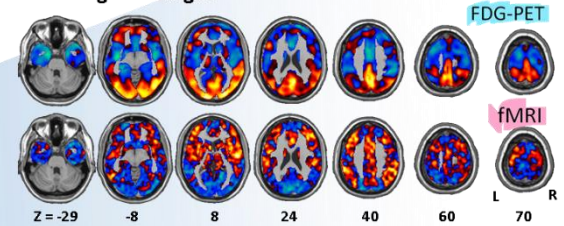
### A. TRAINING DATA SET



### B. TEST DATA SET



### 1<sup>st</sup> singular images



### 2<sup>nd</sup> singular images

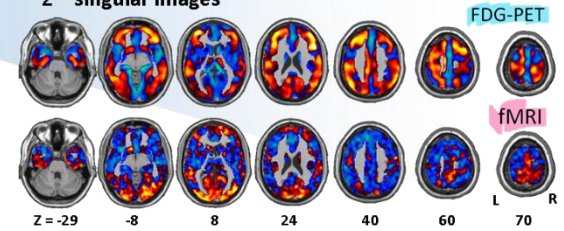


**Figure 6. The spatial covariance patterns between FDG uptake and BOLD signal using a split-half resampling.** (A) The 1<sup>st</sup> and 2<sup>nd</sup> singular images which have maximal relationship between FDG uptake and BOLD signal were significant using the training data set, and (B) using the test data set. Significance was tested using a random permutation test ( $P < 0.005$ ). Each of the singular images accounted for 40.5%, 6.5% of the correlation matrix generated by the training data set, and 34.6%, 13.7% of the correlation matrix generated by the test data set. The percent contribution of each singular image was visualized using scree plot in the middle panel. The significance of singular images was symbolized by a star mark (\*).

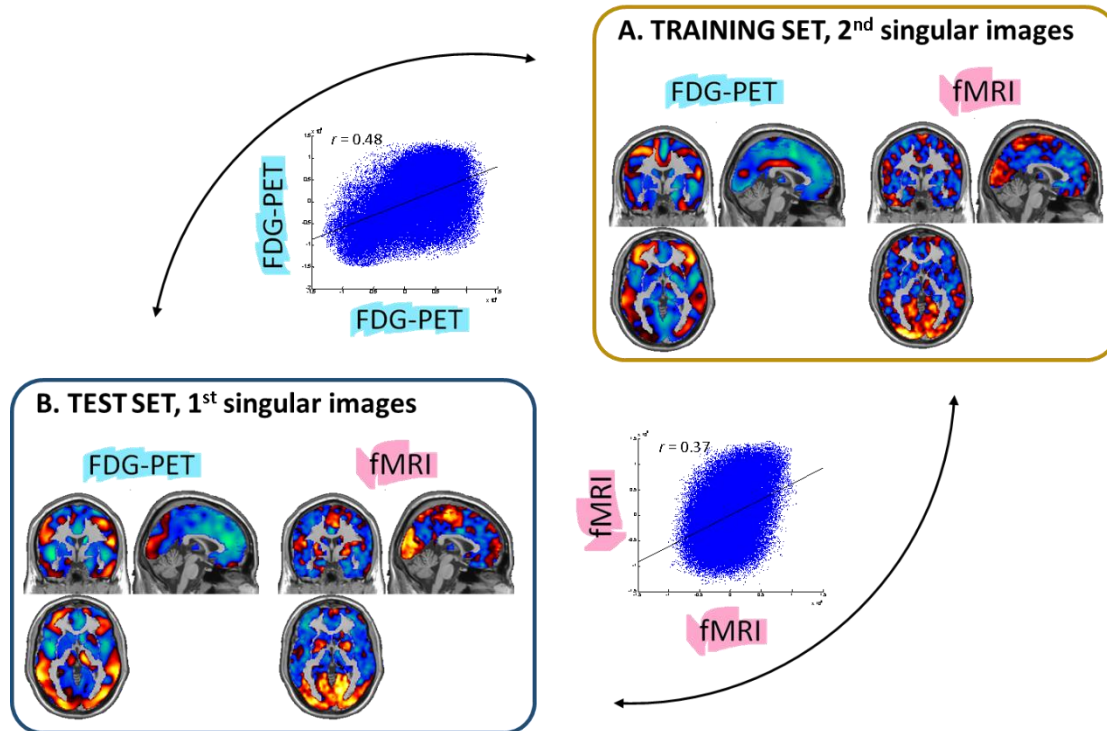


**Figure 7. The reproducibility of the singular images between FDG uptake and BOLD signal using a split-half resampling.** (A) The 2<sup>nd</sup> singular images generated by the training data set were similar to the (B) 1<sup>st</sup> singular images generated by the test data set ( $r = 0.48$  for the FDG-PET, and  $r = 0.37$  for the fMRI). The similarity was measured by the *Pearson's correlation coefficient*.

**Table 2. Reproducibility of the singular images which have maximal relationship between FDG uptake and BOLD signal.** The training data set consisted of half of the participants who were randomly chosen (n=19). The test data set consisted of the other participants (n=19).

			TRAINING DATA SET				TEST DATA SET			
			1 <sup>st</sup> singular image		2 <sup>nd</sup> singular image		1 <sup>st</sup> singular image		2 <sup>nd</sup> singular image	
			PET	fMRI	PET	fMRI	PET	fMRI	PET	fMRI
TRAINING DATA SET	1 <sup>st</sup> singular image	PET fMRI								
	2 <sup>nd</sup> singular image	PET fMRI								
TEST DATA SET	1 <sup>st</sup> singular image	PET fMRI	0.42		0.48					
	2 <sup>nd</sup> singular image	PET fMRI	0.24	-0.28	-0.13	0.37				
				0.14		-0.17				

### 3.3. The principal component images of the FDG-PET and fMRI

The majority of FDG uptake and BOLD signal can be explained by only using a few principal component images (Figure 8A, Figure 9A). Among them, the first three principal component images of FDG-PET significantly explained the FDG uptake at rest (Figure 8B). The first two principal component images of fMRI significantly explained the BOLD signal at rest (Figure 9B).

The 1<sup>st</sup> principal component images of the FDG-PET and fMRI were similar to the 1<sup>st</sup> singular images of the FDG-PET and fMRI, respectively. The similarity between the principal component images and singular images was measured by the *Pearson's* correlation coefficient ( $r = 0.99$  for FDG-PET, see Figure 10A, and  $r = 0.43$  for fMRI, see Figure 11A). In addition, the 2<sup>nd</sup> principal component image of FDG-PET was similar to the 2<sup>nd</sup> singular image of FDG-PET ( $r = 0.88$ , Figure 10B), and the 2<sup>nd</sup> principal component image of fMRI was similar to the 1<sup>st</sup> singular image of fMRI ( $r = 0.56$ , Figure 11B). The 1<sup>st</sup> principal component image of fMRI was also similar to the 2<sup>nd</sup> singular image of fMRI ( $r = 0.96$ , Figure 11C).

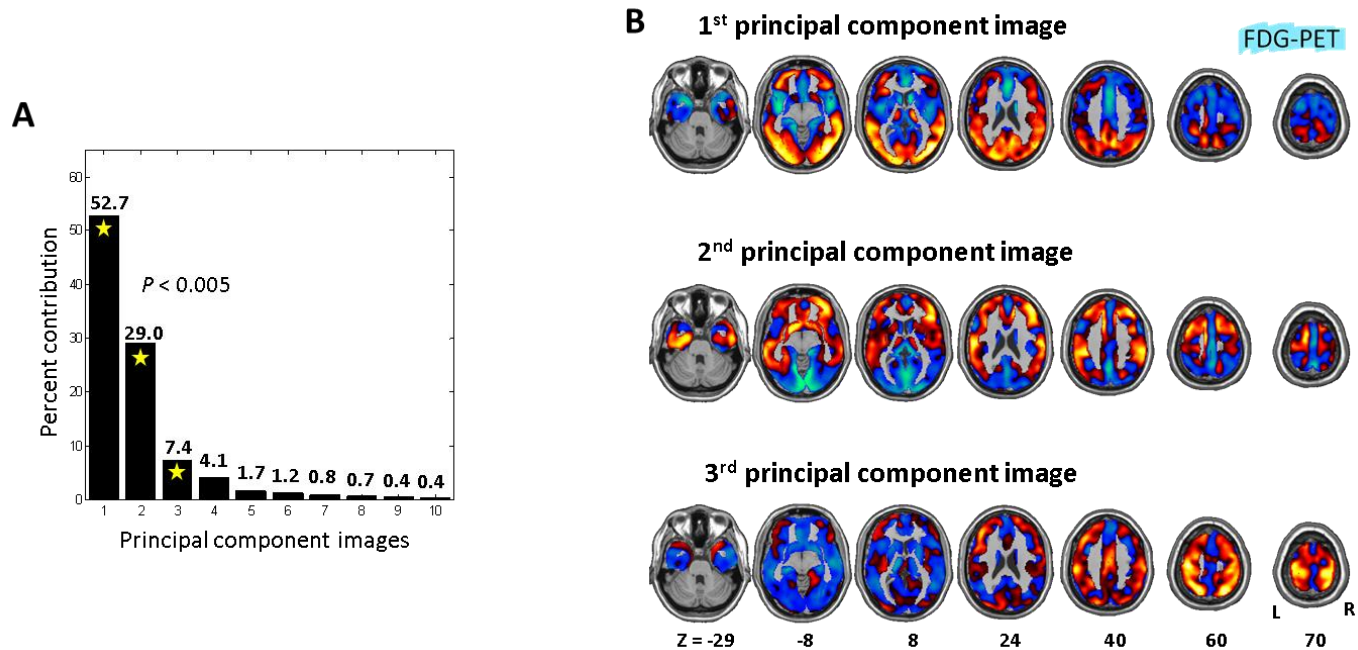


**Figure 8. The percent contribution and visualization of significant principal component images of FDG-PET.** (A) Scree plot in which the percent contribution of the principal component images are ordered from largest to smallest. The x-axis indicate the principal component image index and the y-axis indicate the percent contribution. The significance of principal component images was symbolized by a star mark (\*). (B) The significant principal component images of the FDG-PET.

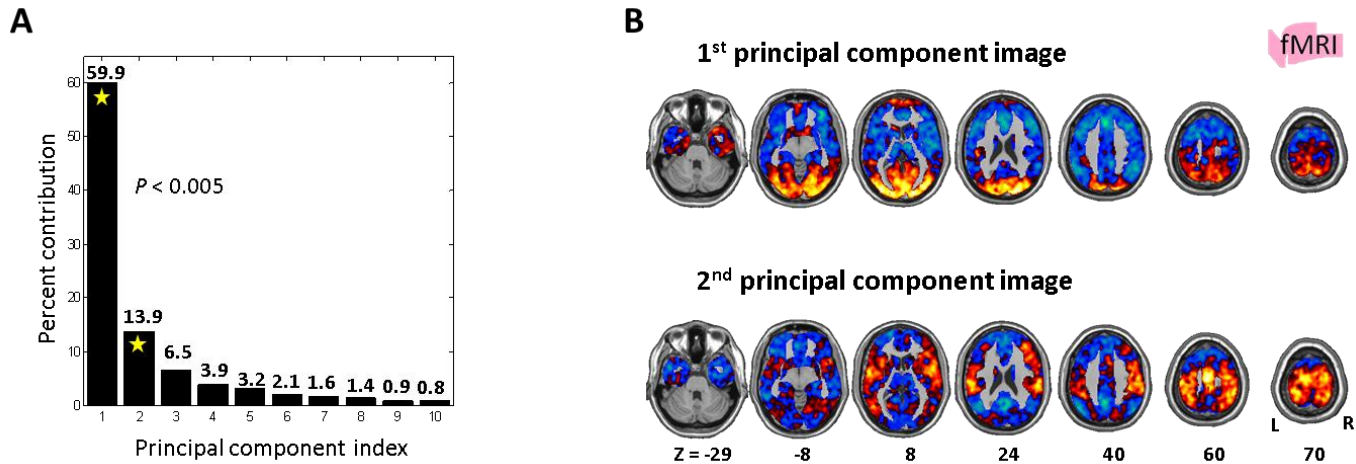
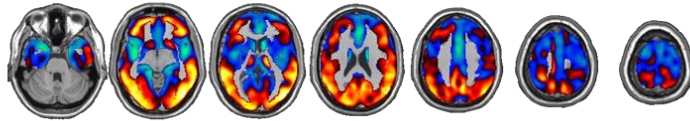
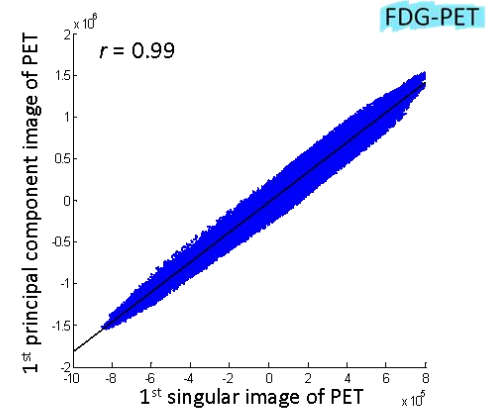
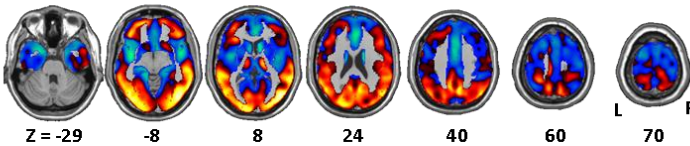


**Figure 9. The percent contribution and visualization of significant principal component images of fMRI.** (A) Scree plot in which the percent contribution of the principal component images are ordered from largest to smallest. The x-axis indicate the principal component image index and the y-axis indicate the percent contribution. The significance of principal component images was symbolized by a star mark (\*). (B) The significant principal component images of the fMRI.

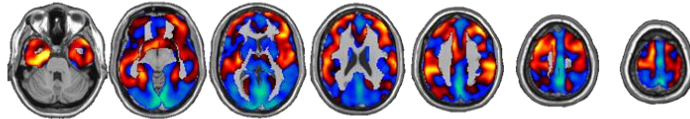
**A** 1<sup>st</sup> singular image (30.4%)



1<sup>st</sup> principal component image (52.7%)



**B** 2<sup>nd</sup> singular image (22.5%)



2<sup>nd</sup> principal component image (29%)

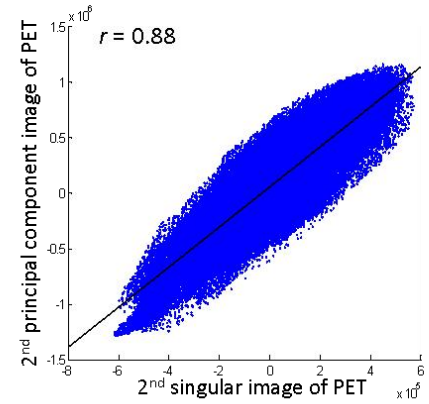
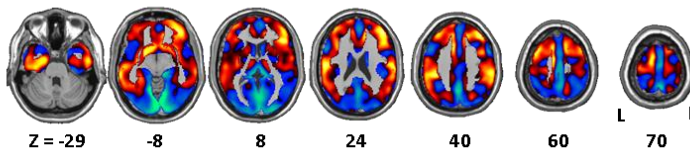


**Figure 10. The agreement between the significant singular images and principal component images of FDG-PET.** (A) The 1<sup>st</sup> singular image of FDG-PET was significantly correlated with the 1<sup>st</sup> principal component image of FDG-PET. (B) The 2<sup>nd</sup> singular image of FDG-PET was significantly correlated with the 2<sup>nd</sup> principal component image of FDG-PET. In the scatter plot, the x-axis indicate the singular image of FDG-PET, and the y-axis indicate the principal component image of FDG-PET.

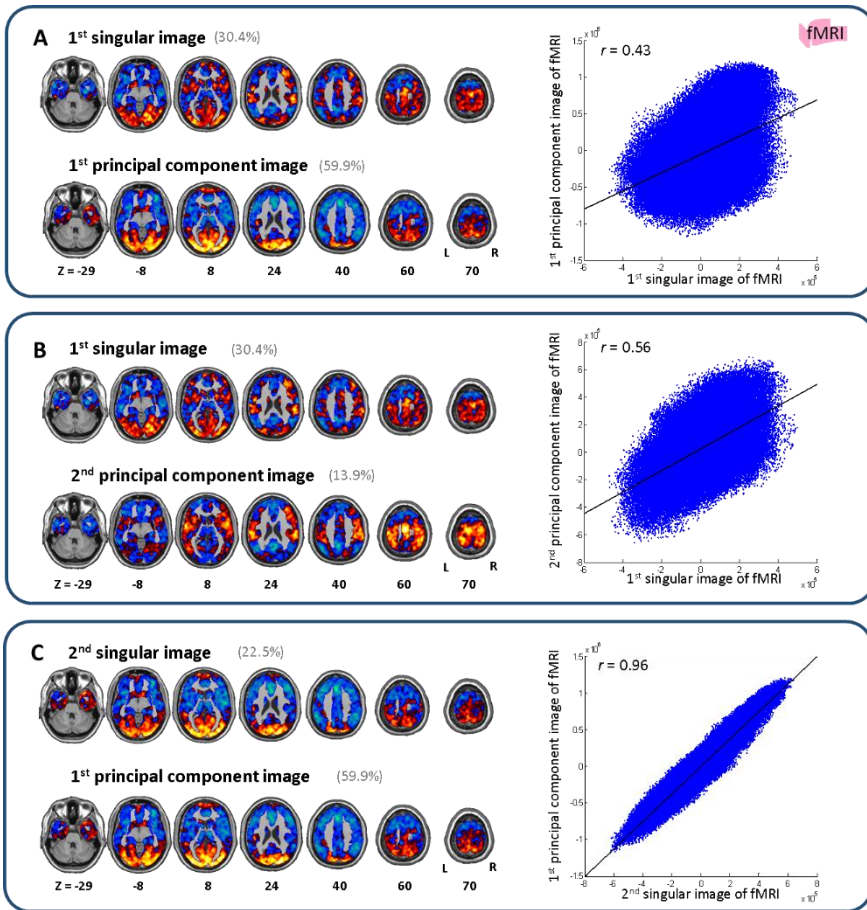


**Figure 11. The agreement between the significant singular images and principal component images of fMRI.** (A) The 1<sup>st</sup> singular image of fMRI was significantly correlated with the 1<sup>st</sup> principal component image of fMRI, and (B) the 2<sup>nd</sup> principal component image of fMRI. (C) The 2<sup>nd</sup> singular image of fMRI was significantly correlated with the 1<sup>st</sup> principal component image of fMRI. In the scatter plot, the x-axis indicate the singular image of fMRI, and the y-axis indicate the principal component image of fMRI.

### **3.4. The effect of age to the significant latent variables**

The relationship between age and 1<sup>st</sup> LV of FDG-PET or 1<sup>st</sup> LV of fMRI was significantly positive ( $r = 0.81$  for FDG-PET, and  $r = 0.69$  for fMRI, Figure 12A). The 1<sup>st</sup> LV was significantly different between the younger adults and older adults groups ( $P = 0.00$  for FDG-PET,  $P = 0.00$  for fMRI, Figure 12B).

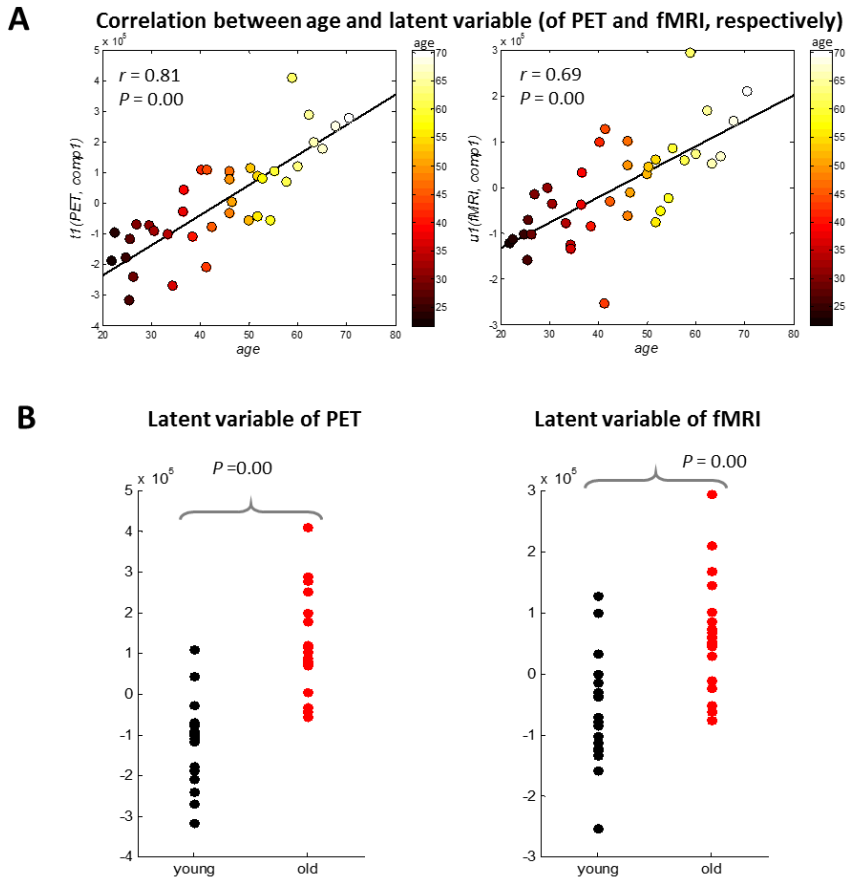


**Figure 12. The relationship between age and FDG uptake or BOLD signal.** (A) The 1<sup>st</sup> LV of FDG-PET and fMRI was positively correlated with age ( $r = 0.81$  for FDG-PET, and  $r = 0.69$  for fMRI). (B) The 1<sup>st</sup> LV was significantly different between the younger adults and older adults groups ( $P = 0.00$  for FDG-PET, and  $P = 0.00$  for fMRI).

### **3.5. The relationship between FDG uptake and BOLD signal in the younger adults and older adults groups.**

In the younger adults group, the spatial covariance patterns which have significant maximal relationship between FDG uptake and BOLD signal were found in the first four components for the FDG-PET and fMRI, respectively ( $P < 0.005$ , Figure 13A). Each of the four singular images accounted for 33.7%, 17.7%, 11.6%, and 8.5% of the correlation matrix.

In the older adults group, the spatial covariance patterns were found in the first two components ( $P < 0.005$ , Figure 13B). Each of the two singular images accounted for 29.5%, and 18.3% of the correlation matrix.

The similarity between the significant singular images of FDG-PET and fMRI were not above the 0.3 at the same time (Table 3), indicating dissimilar relationship between FDG uptake and BOLD signal in the younger adults and older adults groups.

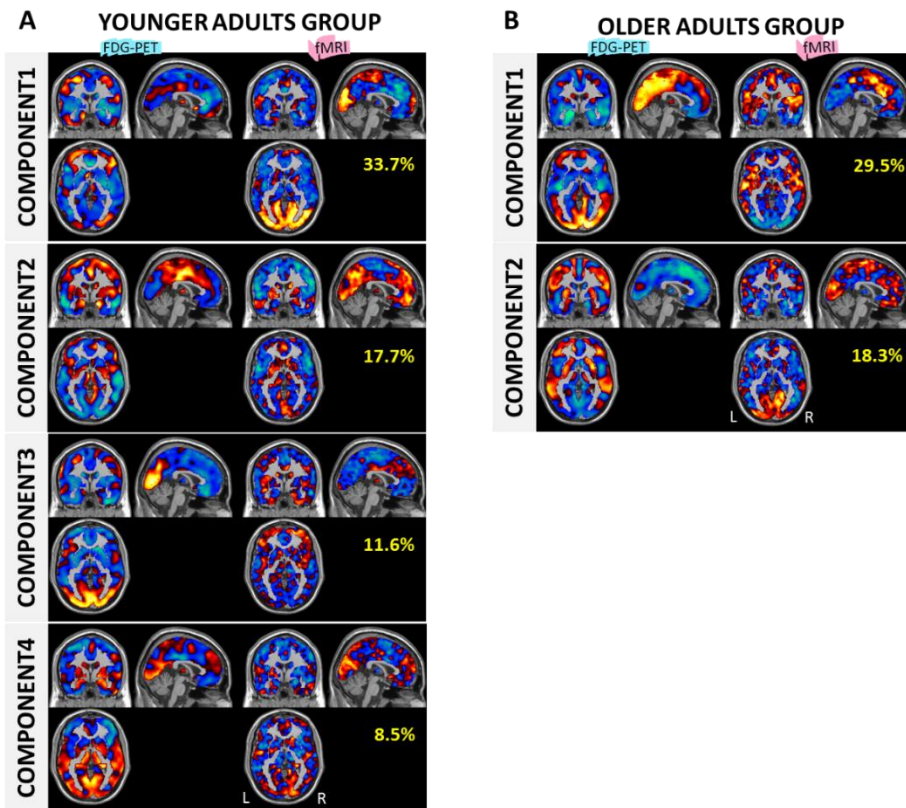


**Figure 13. The spatial covariance patterns between FDG uptake and BOLD signal in the younger adults and older adults groups. (A)** In the younger adults group, the first four singular images showed significant covariance patterns which were not noise, by random permutation test. Each of the four singular images accounted for 33.7%, 17.7%, 11.6%, and 8.5% of the correlation matrix. **(B)** In the older adults group, the first two singular images showed significant covariance patterns which were not noise, by random permutation test. Each of the two singular images accounted for 29.5%, and 18.3% of the correlation matrix.

Table 3. Similarity between the singular images of younger adults and older adults groups, which have maximal relationship between FDG uptake and BOLD signal measured by the *Pearson's* correlation coefficient.

			Younger adults group							
			1 <sup>st</sup> singular image		2 <sup>nd</sup> singular image		3 <sup>rd</sup> singular image		4 <sup>th</sup> singular image	
			PET	fMRI	PET	fMRI	PET	fMRI	PET	fMRI
Older adults group	1 <sup>st</sup> singular image	PET	0.13		0.04		-0.39		0.16	
		fMRI		-0.35		-0.17		-0.01		-0.17
	2 <sup>nd</sup> singular image	PET	0.19		-0.10		0.08		-0.28	
		fMRI		0.17		0.02		0.09		0.11

## **4. Discussion**

Advanced neuroimaging techniques allow investigating human brain in vivo using various imaging modalities. Combining various brain images can help understanding the relationship between brain systems. In this present study, the relationship between FDG uptake and BOLD signal was investigated by using the resting state FDG-PET and fMRI data. Both images were acquired simultaneously using a hybrid PET/MR scanner, although PET images reflected accumulated signal changes before scanning, while fMRI images reflected ongoing signal fluctuation during scanning. The “simultaneous” means that the data was acquired at the same time so they had close temporal proximity. Nevertheless, I can assume that FDG uptake and BOLD signal reflected brain signal at the same time at different points of view, since FDG uptake reflected steady state neural activity, and showed constant continuing level of uptake until the end of the scanning.

### **4.1. Relationship between FDG uptake and BOLD signal at rest**

The spatial pattern of brain representing the significant relationship between resting state FDG uptake and BOLD signal, was found in the first three singular images accounted for 30.4%, 22.5%, and

8.4% of the correlation matrix. The three components described spatially overlapped brain regions. However each component indicated independent and orthogonal relationship between FDG uptake and BOLD signal, by the descending order of singular value. Among them, only the 1<sup>st</sup> singular images were reproducible by a split-half resampling. It indicated that the spatial patterns of brain depicting 2<sup>nd</sup> and 3<sup>rd</sup> singular images might be not found when using different samples.

The spatial pattern was visualized as a pair of brain images in terms of FDG uptake and BOLD signal. The positive and negative weights observed in the pair of brain images represented the distributed network. Theoretically, the positive weight does not indicate higher brain signal. It can be switched to negative weight in different trials. Likewise, the negative weight does not indicate lower brain signal. It can be switched to positive weight in different trials. The important point is their relationship. The significant positive (i.e., showing positive and positive weights or negative and negative weights in the FDG uptake and BOLD signal) and negative relationships (i.e., showing positive and negative weights in the FDG uptake and BOLD signal, and vice versa) were found between FDG-PET and fMRI. The FDG uptake and BOLD signal were interacted with each other, as positive and negative ways at the same time.

From the 1<sup>st</sup> singular images which showed the maximal relationship between FDG uptake and BOLD signal (30.4%), I found that

the FDG uptake of occipito-temporal areas, parietal areas, and lateral frontal areas was (1) positively associated with the BOLD signal of sensory areas including occipital, superior temporal, and pre/postcentral regions. In addition, it was (2) negatively associated with the BOLD signal of default mode network areas. At the same time, the FDG uptake of midline regions of cingulate and frontal areas, and limbic areas was (1) positively associated with the BOLD signal of default mode network areas and ventral temporal areas and (2) negatively associated with the BOLD signal of sensory and motor areas.

The complex relationship indicated that the brain works by combination of different subsystems (Addis et al., 2009; Della-Maggiore et al., 2000). The positive relationship between FDG uptake and BOLD signal observed in the occipito-temporal areas extending to the parietal areas, and lateral frontal areas might be associated with the sensory system in the visual, auditory, and somatosensory regions. At the same time, the positive relationship between FDG uptake and BOLD signal was observed in the default mode network-like system. The FDG uptake observed in the midline regions of cingulate and frontal areas, and limbic areas, and BOLD signal observed in the default mode network areas. In the previous study, the cortical midline structures, integrating with the subcortical midline regions, were suggested as important areas where have a role of self-referential processing (Kjaer et al., 2002; Northoff et

al., 2006). Specifically, the patients with autistic spectrum disorder who had lack of self-reference or self-awareness showed abnormal functional fluctuation in these areas (Lai et al., 2010). These midline cortical structures were closely related to the default-mode network system during resting state condition (D'Argembeau et al., 2005; Whitfield-Gabrieli et al., 2011). The self-referential or self-awareness processing was also related to the default mode network areas (Gusnard et al., 2001; Raichle et al., 2001).

Both two positive relationships described above, were the opposing systems against to each other. The negative relationship between FDG uptake and BOLD signal can be observed between those systems. For example, the FDG uptake of the sensory system was negatively associated with the BOLD signal of the default mode network system, and vice versa. This was a new finding observed between modalities. In the previous study, the negative relationship was observed between the sensory areas and default mode network areas, using resting state fMRI data (Tian et al., 2007).

In line with the relationship observed between modalities, the relationship observed within modality also should be noted. Especially, in the FDG-PET, the posterior cingulate cortex and precuneus, the representative default mode network areas in the previous studies (Fox et al., 2005; Raichle et al., 2001) were negatively associated with the

midline cortical structures. To understand the reason why this contradiction happened, further investigation should be needed. Nevertheless, the dissociated self-referential network of the posterior cingulate cortex to the anterior one (Whitfield-Gabrieli et al., 2011), the integrative role of the precuneus (Cavanna and Trimble, 2006), and the active response to the sensory stimuli of the precuneus (Vogt et al., 1992) might support that the present result was not abnormal. In addition, the default mode network areas including the posterior cingulate cortex and precuneus were not identified by the independent component analysis using FDG-PET data while the midline cortical structures were identified in the same study (Di et al., 2012).

In summary, the positive relationship observed between FDG-PET and fMRI may imply the accommodative interaction of FDG uptake and BOLD signal in healthy adults. The FDG uptake and BOLD signal of the brain areas processing similar functions were related with each other. The negative relationship observed between modalities may also imply the competitive interaction of FDG uptake and BOLD signal.

#### **4.2. The association of the singular images with the principal component images of FDG-PET and fMRI**

The principal component images of FDG-PET and fMRI were

obtained to understand the effect of FDG uptake and BOLD signal to their relationship. In the case of FDG-PET, the 1<sup>st</sup> and 2<sup>nd</sup> principal component images explaining more than 80% of the variance of FDG uptake, were similar to the 1<sup>st</sup> and 2<sup>nd</sup> singular images of FDG-PET derived from the PLS ( $r = 0.99$  and  $r = 0.88$ , respectively). These close associations indicated that the spatial patterns related to the 1<sup>st</sup> and 2<sup>nd</sup> principal component images of FDG-PET were tightly coupled with the resting state BOLD signal. The sensory system and default mode network-like system were observed in the principal component images of FDG-PET.

In the case of fMRI, the 1<sup>st</sup> and 2<sup>nd</sup> principal component images explaining more than 70% of the variance of BOLD signal, were similar to the 1<sup>st</sup> singular image of fMRI derived from the PLS ( $r = 0.43$  and  $r = 0.56$ , respectively). The 1<sup>st</sup> principal component image represented the visual system and default mode network system while the 2<sup>nd</sup> principal component image represented the auditory/motor system, and default mode network system. The principal component images of fMRI represented the specialized brain systems separately, compared to the FDG-PET.

The BOLD signal at rest reflected the spontaneous, ongoing neural activity. The temporal dynamics led to large variance between brain signals which were susceptible to construct brain networks.

Therefore the distinctive interregional correlation patterns were observed more by using the BOLD signal than using the FDG uptake. The two principal component images of fMRI contributing to the relationship of FDG uptake indicated the specialized brain systems, to balance the brain energy demands and transient neural activity.

In summary, the 1<sup>st</sup> principal component image of FDG-PET was closely coupled with the 1<sup>st</sup> and 2<sup>nd</sup> principal component images of fMRI. The 2<sup>nd</sup> principal component image of FDG-PET was closely coupled with the 1<sup>st</sup> principal component image of fMRI. The close coupling was proved to be the best, which captures the maximal relationship between modalities by the PLS. In other words, the FDG uptake and BOLD signal represented by the principal component images were wired together to function complementarily to each other.

### **4.3. The effect of age to the relationship between FDG uptake and BOLD signal**

The present results illustrated the relationship between FDG uptake and BOLD signal, but the physiological meaning of the results remained unknown. Interestingly, the 1<sup>st</sup> latent variables of FDG-PET and fMRI were correlated with age, and were different between younger adults and older adults groups (Figure 12). The results proved that the

relationship between FDG uptake and BOLD signal was changed by age. According to the results, I set up the analyses to investigate the effect of age to the relationship between the FDG uptake and BOLD signal.

In the younger adults group, the significant relationship was found in the first four singular images. While in the older adults group, the significant relationship was found in the first two singular images. There was no agreement of singular images between the groups by the Pearson's correlation coefficient ( $r < 0.3$ ). It indicated that the relationship between FDG uptake and BOLD signal was dissimilar between groups. Since there was no statistical parameters to compare the changes of the relationship between groups, I described the results focusing on the 1<sup>st</sup> singular images, which best explained the relationship (33.7% correlation was explained in the younger adults group, and 29.5% correlation was explained in the older adults group). In the younger adults group, spatially similar areas showed positive relationship between FDG uptake and BOLD signal, like the result of whole group analysis. In the older adults group, however, spatially similar areas showed negative relationship between FDG uptake and BOLD signal.

This shifted relationship observed between modalities suggested that the brain of older adults works differently, and age was the main factor inducing the shifted relationship. Considering the FDG uptake and

BOLD signal in an integrated perspective can help to shed light on how the brain works.

## **5. Conclusion and limitations**

This study proposed a new insight about the relationship between FDG uptake and BOLD signal at rest using bimodal and multivariate partial least squares analysis. The positive and negative relationships were observed different brain regions in respect to their functional processing and were changed by age. The FDG uptake and BOLD signal were wired together complementarily, which was revealed by the principal component images depicting the interregional correlation within modality and by the singular images depicting the relationship between modalities.

In this study, the brain signal was measured simultaneously by using a hybrid PET/MR scanner, allowing acquisition of FDG-PET and functional MR images in identical person, under the close temporal proximity between different image modalities. Investigating FDG uptake and BOLD signal in identical person helps to avoid inter-individual and inter-scan variability. The another advantage of this study was no need for correcting multiple comparisons since no statistical test was performed to test the significance of singular images by the PLS method (McIntosh and Lobaugh, 2004). The significance of each singular image was tested by a permutation method. The statistical inference was not a voxel but the singular image corresponding to the singular value itself.

Also, the interdependency between voxels which may affect to the relationship between FDG uptake and BOLD signal was considered by the PLS.

Unlike the previous studies, the relationship between FDG uptake and BOLD signal was not always positive but complex to interpret. I have carefully discussed some possible explanations leading to the relationship between modalities. However, some shortcomings also should be mentioned. The physiological meaning of the relationship was obscured although there was a close coupling between FDG uptake and BOLD signal. In addition, in this present work, the number of sample was too small compared to the large number of voxels, to obtain statistically meaningful results of the cross-validation tests. Also, the criteria of age was 45 for distinguishing the older adults group from the younger adults group. According to the previous studies, the changes of cerebellar volume with age showed inverted U-shape at the ages of 40s (Raz et al., 2005), and the turning point of dopamine transporter uptake across the lifespan occurred at the ages of late 30s and 40s (Mozley et al., 1999). However the participants of this study may not be representative of younger adults and older adults groups compared to the previous studies using extreme group contrast (20-30s for younger adults group, and 60-70s for older adults group) (Cabeza et al., 2002; Grady et al., 1994) to find evidence proving group differences. The trajectories of

lifespan changes on brain may be more understandable by including the ‘middle age (40-50s) group’ for investigating age effect to the brain (Grady et al., 2006; Kennedy et al., 2015). The ‘emerging adults’ distinguishing the early younger adults group from the others (Bennett and Baird, 2006) also should be appropriate for future studies using a large number of samples.

Nevertheless, the hypotheses about the relationship between FDG uptake and BOLD signal, and the effect of age were reasonable. The relationship between FDG uptake and BOLD signal might be essential in healthy adults to maintain normal brain function. Therefore, the people who showed impaired FDG uptake or abnormal BOLD fluctuation might have significantly altered relationship between FDG uptake and BOLD signal. Investigating Alzheimer’s patients and schizophrenia can help to support this interpretation. The effect of age to the relationship should have been discussed thoroughly using a large number of sample. In addition, representative measurement reflecting the relationship between FDG uptake and BOLD signal should be needed in future studies.

## References

- Addis, D.R., Pan, L., Vu, M.-A., Laiser, N., Schacter, D.L. 2009. Constructive episodic simulation of the future and the past: Distinct subsystems of a core brain network mediate imagining and remembering. *Neuropsychologia* 47, 2222-2238.
- Bélangier, M., Allaman, I., Magistretti, Pierre J. 2011. Brain Energy Metabolism: Focus on Astrocyte-Neuron Metabolic Cooperation. *Cell Metabolism* 14, 724-738.
- Bennett, C.M., Baird, A.A. 2006. Anatomical changes in the emerging adult brain: a voxel-based morphometry study. *Hum Brain Mapp* 27, 766-77.
- Boellaard, R., O'Doherty, M.J., Weber, W.A., Mottaghy, F.M., Lonsdale, M.N., Stroobants, S.G., Oyen, W.J., Kotzerke, J., Hoekstra, O.S., Pruim, J. 2010. FDG PET and PET/CT: EANM procedure guidelines for tumour PET imaging: version 1.0. *Eur J Nucl Med Mol Imaging* 37, 181-200.
- Burzynska, A.Z., Garrett, D.D., Preuschhof, C., Nagel, I.E., Li, S.C., Backman, L., Heekeren, H.R., Lindenberger, U. 2013. A scaffold for efficiency in the human brain. *J Neurosci* 33, 17150-9.
- Cabeza, R., Anderson, N.D., Locantore, J.K., McIntosh, A.R. 2002. Aging gracefully: compensatory brain activity in high-performing older adults. *Neuroimage* 17, 1394-402.
- Calhoun, V.D., Adali, T., Kiehl, K.A., Astur, R., Pekar, J.J., Pearlson, G.D. 2006. A method for multitask fMRI data fusion applied to schizophrenia. *Hum Brain Mapp* 27, 598-610.
- Cavanna, A.E., Trimble, M.R. 2006. The precuneus: a review of its functional anatomy and behavioural correlates. *Brain* 129, 564-583.
- Chen, K., Reiman, E.M., Huan, Z., Caselli, R.J., Bandy, D., Ayutyanont, N., Alexander, G.E. 2009. Linking functional and structural brain images with multivariate network analyses: A novel application of the partial least square method. *Neuroimage* 47, 602-610.
- Cohen, J. *Statistical power analysis for the behavioral sciences*. 1988, 2nd ed Hillsdale. NJ Lawrence Earlbaum Associates.

- Correa, N.M., Eichele, T., Adali, T., Li, Y.O., Calhoun, V.D. 2010. Multi-set canonical correlation analysis for the fusion of concurrent single trial ERP and functional MRI. *Neuroimage* 50, 1438-45.
- Cox, R.W. 1996. AFNI: Software for Analysis and Visualization of Functional Magnetic Resonance Neuroimages. *Comput Biomed Res* 29, 162-173.
- D'Argembeau, A., Collette, F., Van der Linden, M., Laureys, S., Del Fiore, G., Degueldre, C., Luxen, A., Salmon, E. 2005. Self-referential reflective activity and its relationship with rest: a PET study. *Neuroimage* 25, 616-624.
- Della-Maggiore, V., Sekuler, A.B., Grady, C.L., Bennett, P.J., Sekuler, R., McIntosh, A.R. 2000. Corticolimbic interactions associated with performance on a short-term memory task are modified by age. *J Neurosci* 20, 8410-6.
- Di, X., Biswal, Alzheimer's Disease Neuroimaging Initiative, B.B. 2012. Metabolic brain covariant networks as revealed by FDG-PET with reference to resting-state fMRI networks. *Brain connectivity* 2, 275-283.
- Ferreira, L.K., Busatto, G.F. 2013. Resting-state functional connectivity in normal brain aging. *Neurosci Biobehav Rev* 37, 384-400.
- Fox, M.D., Snyder, A.Z., Vincent, J.L., Corbetta, M., Van Essen, D.C., Raichle, M.E. 2005. The human brain is intrinsically organized into dynamic, anticorrelated functional networks. *Proc Natl Acad Sci U S A* 102, 9673-9678.
- Franco, A.R., Ling, J., Caprihan, A., Calhoun, V.D., Jung, R.E., Heileman, G.L., Mayer, A.R. 2008. Multimodal and Multi-tissue Measures of Connectivity Revealed by Joint Independent Component Analysis. *IEEE J Sel Top Signal Process* 2, 986-997.
- Friston, K.J., Frith, C.D., Liddle, P.F., Frackowiak, R.S. 1993. Functional connectivity: the principal-component analysis of large (PET) data sets. *J Cereb Blood Flow Metab* 13, 5-14.
- Grady, C., Springer, M., Hongwanishkul, D., McIntosh, A., Winocur, G. 2006. Age-related changes in brain activity across the adult lifespan. *Cognitive Neuroscience, Journal of* 18, 227-241.
- Grady, C.L., Maisog, J.M., Horwitz, B., Ungerleider, L.G., Mentis, M.J.,

- Salerno, J.A., Pietrini, P., Wagner, E., Haxby, J.V. 1994. Age-related changes in cortical blood flow activation during visual processing of faces and location. *J Neurosci* 14, 1450-62.
- Gusnard, D.A., Raichle, M.E., Raichle, M.E. 2001. Searching for a baseline: functional imaging and the resting human brain. *Nat Rev Neurosci* 2, 685-94.
- Hasson, U., Nusbaum, H.C., Small, S.L. 2009. Task-dependent organization of brain regions active during rest. *Proc Natl Acad Sci U S A* 106, 10841-6.
- Heiss, W.-D. 2009. The potential of PET/MR for brain imaging. *Eur J Nucl Med Mol Imaging* 36, 105-112.
- Hertz, L., Zielke, H.R. 2004. Astrocytic control of glutamatergic activity: astrocytes as stars of the show. *Trends Neurosci* 27, 735-43.
- Horwitz, B., Poeppel, D. 2002. How can EEG/MEG and fMRI/PET data be combined? *Hum Brain Mapp* 17, 1-3.
- Huster, R.J., Debener, S., Eichele, T., Herrmann, C.S. 2012. Methods for simultaneous EEG-fMRI: an introductory review. *J Neurosci* 32, 6053-60.
- Hyder, F., Rothman, D.L., Shulman, R.G. 2002. Total neuroenergetics support localized brain activity: implications for the interpretation of fMRI. *Proc Natl Acad Sci U S A* 99, 10771-6.
- Hyder, F., Herman, P., Sanganahalli, B.G., Coman, D., Blumenfeld, H., Rothman, D.L. 2011. Role of ongoing, intrinsic activity of neuronal populations for quantitative neuroimaging of functional magnetic resonance imaging-based networks. *Brain Connect* 1, 185-93.
- Iannaccone, R., Hauser, T.U., Staempfli, P., Walitza, S., Brandeis, D., Brem, S. 2015. Conflict monitoring and error processing: New insights from simultaneous EEG-fMRI. *Neuroimage* 105, 395-407.
- Jenkinson, M., Bannister, P., Brady, M., Smith, S. 2002. Improved Optimization for the Robust and Accurate Linear Registration and Motion Correction of Brain Images. *Neuroimage* 17, 825-841.
- Jo, H.J., Gotts, S.J., Reynolds, R.C., Bandettini, P.A., Martin, A., Cox,

- R.W., Saad, Z.S. 2013. Effective Preprocessing Procedures Virtually Eliminate Distance-Dependent Motion Artifacts in Resting State fMRI. *J Appl Math* 2013.
- Kennedy, K.M., Rodrigue, K.M., Bischof, G.N., Hebrank, A.C., Reuter-Lorenz, P.A., Park, D.C. 2015. Age trajectories of functional activation under conditions of low and high processing demands: An adult lifespan fMRI study of the aging brain. *Neuroimage* 104, 21-34.
- Kjaer, T.W., Nowak, M., Lou, H.C. 2002. Reflective self-awareness and conscious states: PET evidence for a common midline parietofrontal core. *Neuroimage* 17, 1080-6.
- Krishnan, A., Williams, L.J., McIntosh, A.R., Abdi, H. 2011. Partial Least Squares (PLS) methods for neuroimaging: a tutorial and review. *Neuroimage* 56, 455-75.
- Lai, M.-C., Lombardo, M.V., Chakrabarti, B., Sadek, S.A., Pasco, G., Wheelwright, S.J., Bullmore, E.T., Baron-Cohen, S., Suckling, J., Consortium, M.A. 2010. A shift to randomness of brain oscillations in people with autism. *Biol Psychiatry* 68, 1092-1099.
- Lewis, C.M., Baldassarre, A., Committeri, G., Romani, G.L., Corbetta, M. 2009. Learning sculpts the spontaneous activity of the resting human brain. *Proc Natl Acad Sci U S A* 106, 17558-63.
- McIntosh, A., Bookstein, F., Haxby, J.V., Grady, C. 1996. Spatial pattern analysis of functional brain images using partial least squares. *Neuroimage* 3, 143-157.
- McIntosh, A.R., Lobaugh, N.J. 2004. Partial least squares analysis of neuroimaging data: applications and advances. *Neuroimage* 23, Supplement 1, S250-S263.
- Menon, V., Ford, J.M., Lim, K.O., Glover, G.H., Pfefferbaum, A. 1997. Combined event-related fMRI and EEG evidence for temporal—parietal cortex activation during target detection. *Neuroreport* 8, 3029-3037.
- Milan, L., Whittaker, J. 1995. Application of the parametric bootstrap to models that incorporate a singular value decomposition. *Applied Statistics*, 31-49.
- Moosmann, M., Eichele, T., Nordby, H., Hugdahl, K., Calhoun, V.D.

2008. Joint independent component analysis for simultaneous EEG–fMRI: Principle and simulation. *Int J Psychophysiol* 67, 212-221.
- Mozley, P.D., Acton, P.D., Barraclough, E.D., Plössl, K., Gur, R.C., Alavi, A., Mathur, A., Saffer, J., Kung, H.F. 1999. Effects of age on dopamine transporters in healthy humans. *Journal of nuclear medicine: official publication, Society of Nuclear Medicine* 40, 1812-1817.
- Mulert, C., Jäger, L., Schmitt, R., Bussfeld, P., Pogarell, O., Möller, H.-J., Juckel, G., Hegerl, U. 2004. Integration of fMRI and simultaneous EEG: towards a comprehensive understanding of localization and time-course of brain activity in target detection. *Neuroimage* 22, 83-94.
- Muller-Gartner, H.W., Links, J.M., Prince, J.L., Bryan, R.N., McVeigh, E., Leal, J.P., Davatzikos, C., Frost, J.J. 1992. Measurement of radiotracer concentration in brain gray matter using positron emission tomography: MRI-based correction for partial volume effects. *J Cereb Blood Flow Metab* 12, 571-83.
- Newberg, A.B., Wang, J., Rao, H., Swanson, R.L., Wintering, N., Karp, J.S., Alavi, A., Greenberg, J.H., Detre, J.A. 2005. Concurrent CBF and CMRGlc changes during human brain activation by combined fMRI-PET scanning. *Neuroimage* 28, 500-6.
- Northoff, G., Heinzl, A., de Greck, M., Bermpohl, F., Dobrowolny, H., Panksepp, J. 2006. Self-referential processing in our brain—A meta-analysis of imaging studies on the self. *Neuroimage* 31, 440-457.
- Nugent, A.C., Martinez, A., D'Alfonso, A., Zarate, C.A., Theodore, W.H. 2015. The relationship between glucose metabolism, resting-state fMRI BOLD signal, and GABAA-binding potential: a preliminary study in healthy subjects and those with temporal lobe epilepsy. *J Cereb Blood Flow Metab*.
- Ogawa, S., Lee, T.M., Kay, A.R., Tank, D.W. 1990. Brain magnetic resonance imaging with contrast dependent on blood oxygenation. *Proc Natl Acad Sci U S A* 87, 9868-72.
- Ogawa, S., Menon, R., Tank, D., Kim, S., Merkle, H., Ellermann, J., Ugurbil, K. 1993. Functional brain mapping by blood oxygenation level-dependent contrast magnetic resonance

imaging. A comparison of signal characteristics with a biophysical model. *Biophys J* 64, 803-812.

Passow, S., Specht, K., Adamsen, T.C., Biermann, M., Brekke, N., Craven, A.R., Ersland, L., Grüner, R., Kleven-Madsen, N., Kvernenes, O.H. 2015. Default-mode network functional connectivity is closely related to metabolic activity. *Hum Brain Mapp.*

Power, J.D., Barnes, K.A., Snyder, A.Z., Schlaggar, B.L., Petersen, S.E. 2012. Spurious but systematic correlations in functional connectivity MRI networks arise from subject motion. *Neuroimage* 59, 2142-2154.

Quarantelli, M., Berkouk, K., Prinster, A., Landeau, B., Svarer, C., Balkay, L., Alfano, B., Brunetti, A., Baron, J.C., Salvatore, M. 2004. Integrated software for the analysis of brain PET/SPECT studies with partial-volume-effect correction. *J Nucl Med* 45, 192-201.

Raichle, M.E. 1998. Behind the scenes of functional brain imaging: a historical and physiological perspective. *Proc Natl Acad Sci U S A* 95, 765-72.

Raichle, M.E. 2009. A brief history of human brain mapping. *Trends Neurosci* 32, 118-26.

Raichle, M.E. 2010. Two views of brain function. *Trends Cogn Sci* 14, 180-90.

Raichle, M.E., MacLeod, A.M., Snyder, A.Z., Powers, W.J., Gusnard, D.A., Shulman, G.L. 2001. A default mode of brain function. *Proc Natl Acad Sci U S A* 98, 676-82.

Raz, N., Lindenberger, U., Rodrigue, K.M., Kennedy, K.M., Head, D., Williamson, A., Dahle, C., Gerstorf, D., Acker, J.D. 2005. Regional brain changes in aging healthy adults: general trends, individual differences and modifiers. *Cereb Cortex* 15, 1676-1689.

Riedl, V., Bienkowska, K., Strobel, C., Tahmasian, M., Grimmer, T., Forster, S., Friston, K.J., Sorg, C., Drzezga, A. 2014. Local activity determines functional connectivity in the resting human brain: a simultaneous FDG-PET/fMRI study. *J Neurosci* 34, 6260-6.

- Rousset, O.G., Ma, Y., Evans, A.C. 1998. Correction for partial volume effects in PET: principle and validation. *J Nucl Med* 39, 904-11.
- Schmidt, K.C., Lucignani, G., Sokoloff, L. 1996. Fluorine-18-fluorodeoxyglucose PET to determine regional cerebral glucose utilization: A re-examination. *J Nucl Med* 37, 394-399.
- Shulman, R.G., Hyder, F., Rothman, D.L. 2002. Biophysical basis of brain activity: implications for neuroimaging. *Q Rev Biophys* 35, 287-325.
- Shulman, R.G., Rothman, D.L., Behar, K.L., Hyder, F. 2004. Energetic basis of brain activity: implications for neuroimaging. *Trends Neurosci* 27, 489-95.
- Smith, S.M., Jenkinson, M., Woolrich, M.W., Beckmann, C.F., Behrens, T.E., Johansen-Berg, H., Bannister, P.R., De Luca, M., Drobnjak, I., Flitney, D.E., Niazy, R.K., Saunders, J., Vickers, J., Zhang, Y., De Stefano, N., Brady, J.M., Matthews, P.M. 2004. Advances in functional and structural MR image analysis and implementation as FSL. *Neuroimage* 23 Suppl 1, S208-19.
- Strelnikov, K. 2010. Neuroimaging and neuroenergetics: Brain activations as information-driven reorganization of energy flows. *Brain Cogn* 72, 449-456.
- Sui, J., Adali, T., Yu, Q., Chen, J., Calhoun, V.D. 2012. A review of multivariate methods for multimodal fusion of brain imaging data. *J Neurosci Methods* 204, 68-81.
- Tian, L., Jiang, T., Liu, Y., Yu, C., Wang, K., Zhou, Y., Song, M., Li, K. 2007. The relationship within and between the extrinsic and intrinsic systems indicated by resting state correlational patterns of sensory cortices. *Neuroimage* 36, 684-690.
- Tomasi, D., Wang, G.J., Volkow, N.D. 2013. Energetic cost of brain functional connectivity. *Proc Natl Acad Sci U S A* 110, 13642-7.
- Vogt, B.A., Finch, D.M., Olson, C.R. 1992. Functional heterogeneity in cingulate cortex: the anterior executive and posterior evaluative regions. *Cereb Cortex* 2, 435-443.
- Wehrl, H.F., Wiehr, S., Divine, M.R., Gatidis, S., Gullberg, G.T., Maier, F.C., Rolle, A.M., Schwenck, J., Thaiss, W.M., Pichler, B.J. 2014. Preclinical and Translational PET/MR Imaging. *J Nucl Med* 55,

11S-18S.

- Whitfield-Gabrieli, S., Moran, J.M., Nieto-Castañón, A., Triantafyllou, C., Saxe, R., Gabrieli, J.D.E. 2011. Associations and dissociations between default and self-reference networks in the human brain. *Neuroimage* 55, 225-232.
- Worsley, K.J., Chen, J.-I., Lerch, J., Evans, A.C. 2005. Comparing functional connectivity via thresholding correlations and singular value decomposition. *Philosophical Transactions of the Royal Society B: Biological Sciences* 360, 913-920.

국문 초록

휴지기 뇌 포도당 대사와  
BOLD 신호 관계에 관한  
다중모달리티 다변량 분석법:  
하이브리드 PET/MR 연구

김은경

협동과정 인지과학 전공

서울대학교 대학원

휴지기 뇌 포도당 소비량과 뇌 신경 활동에 따른 혈류의 반응은 일반적으로 뇌의 내재적 기능을 반영한다. 뇌가 어떻게 기능하는가를 더 잘 이해하기 위해서는 이들의 관계를 연구하는 것이 필수적이다. 본 연구는 하이브리드 PET/MR 장비를 사용해서 뇌 기능의 서로 다른 측면을 반영하는 포도당 대사와 BOLD 신호의 관계를 알아보고자 다변량 통계분석법 중 하나인 partial least squares 방법을 적용했다(총 38명, 평균 나이  $44 \pm 13.9$ 세). 이 방법으로 뇌 복셀(voxel) 간 상호의존성과 모달리티 간 관계를 함께 고려할 수 있다.

분석 결과, 서로 다른 기능을 하는 영역에서 뇌 포도당 대사와 BOLD 신호의 관계를 관찰하였고 split-half resampling을 통해 다른 집단에서도 이 관계가 관찰 가능함을 확인하였다. 예를 들어 (1) 감각(sensory) 시스템과 (2) 디폴트 모드 시스템(default mode network-like)에서 포도당 대사와 BOLD 신호의 정적인 상관관계를 관찰하였다. 또한 위의 감각 처리 관련 영역과 디폴트 모드 연결망 관련 영역에서 뇌 포도당 대사와 BOLD 신호의 부적인 상관관계를 관찰하였다.

또한 본 연구에서는 각 모달리티의 영역간 상관을 알아보기 위해서 주성분 분석을 실시하였다. FDG-PET의 첫 번째 주성분 이미지는 뇌 포도당 대사와 BOLD 신호의 관계에서 관찰된 FDG-PET의 첫 번째 특이값 이미지(singular image)와 유사했다. 반면에 fMRI의 첫 번째, 두 번째 주성분 이미지는 뇌 포도당 대사와 BOLD 신호의 관계에서 관찰된 fMRI의 첫 번째 특이값 이미지와 유사했다. fMRI의 첫 번째 주성분은 (1) 시각(visual) 시스템과 (2) 디폴트 모드 시스템을 보여주고 있다. fMRI의 두 번째 주성분은 (1) 청각(auditory) 시스템과 운동(motor) 시스템, 그리고 (2) 디폴트 모드 시스템을 보여주고 있다. 이는 fMRI로 측정된 신경신호로부터 계산된 영역간 상관이 PET과 달리 시각과 청각/운동 시스템을 기능적으로 독립된 시스템으로 구분하고 있음을 의미한다.

본 연구 결과 뇌 포도당 대사와 BOLD 신호의 관계는 나이에 따라 변화하는 것으로 보인다. 젊은 성인(총 19명, 평균 나이  $32 \pm 6.9$ 세)과 중년 성인(총 19명, 평균 나이  $56 \pm 7.7$ 세) 집단으로 나누어 partial least squares를 적용한 결과, 나이에 따라 뇌 포도당 대사와 BOLD 신호의 관계가 달라짐을 관찰하였다. 노화에 따른 뇌기능의 변화는 뇌 포도당 대사와 BOLD 신호 간 관계의 변화를 통해서도

관찰할 수 있다.

**주요어:** FDG-PET, 휴지기 fMRI, partial least squares, 다중영상, 하이브리드 PET/MR, 나이

**학번:** 2011-30865